Synthesis and Characterization of ZnO Nanoparticles for Potential Application in Photocatalysis

By

Aqsa Aziz

School of Chemical and Materials Engineering (SCME)

National University of Sciences and Technology (NUST)

2018

Synthesis and Characterization of ZnO Nanoparticles for Potential Application in Photocatalysis

Names: Aqsa Aziz

Reg. No: 117934

This thesis is submitted as a partial fulfillment of the requirements for the degree of

MS in Nanoscience and Engineering

Supervisor Name: Dr. Umair Manzoor

School of Chemical and Materials Engineering (SCME)

National University of Sciences and Technology (NUST)

H-12 Islamabad, Pakistan

November, 2018

This work is dedicated to

my Parents

for their eternal love and support,

my Siblings

especially my younger sister

Dr. Iqra Aziz

for her assistance whenever I needed,

and because I know seeing this would always bring a smile to her face for, she loved the idea of her name being written here

and

my Friends

for adding colors in my life.

Acknowledgements

All commendations be to Allah, the beneficent and Merciful, who made us in the Muslim Ummah. I am profoundly grateful to Allah Almighty for issuing me the wisdom, strength, courage and vision to finish this work.

I would like to express my profound gratitude to my supervisor Dr. Umair Manzoor, for his support throughout this research. His keen interest and incessant optimism have been constant source of encouragement which continuously motivated me in trying to excel in my work. I am extremely thankful to him for taking out his time in listening to my queries and showing immense patience with my work. This thesis wouldn't have been possible without his guidance and dedication.

My sincere thanks to the Principal SCME, for giving me the opportunity and providing me with a platform with all needed facilities. I express emphatic gratitude to Dr. Muhammad Israr Qadir for introducing me to zinc oxide (ZnO), the topic of my research. I would like to acknowledge my GEC committee Dr. Mohammad Mujahid and Zakir Hussain for their support. I am truly obliged to Dr. Muhammad Aftab Akram for having willingly shared his precious time for discussions and Dr. Sofia Javed for allowing me access to Nano lab and use of related equipment. I appreciate assistance from all other faculty members of Materials as well as Chemical Department, furthermore, the lab and NG staff members for their help in every manner.

Special thanks to Dr. Iftikhar Ahmad for TEM characterization of samples at Center of Excellence for Research in Engineering Materials (CEREM), King Saud University, Riyadh and Dr. Awais Ali for Photoluminesce characterization of samples at Centre for Micro and Nano Devices (CMND), COMSATS, Islamabad.

Last but not the least, I am forever grateful to my parents for allowing me to pursue my dreams. I am truly blessed in terms of family and friends, who supported me through thick and thin.

Aqsa Aziz

Abstract

Zinc oxide (ZnO) is one of the most promising semiconducting material in the field of photo-catalysis due to its optical and electrical properties. This work is based on synthesis of ZnO nanoparticles through modified coprecipitation technique. The growth conditions were controlled via carefully designed oil bath and reflux setup. The study explored the effect of acetate, sulfate and nitrate salt precursors along with synthesis temperature on physiochemical behavior of ZnO nanoparticles. XRD and SEM analysis confirmed phase pure hexagonal wurtzite zinc oxide nanoparticles of spherical morphology ranging from 30nm to 70nm in size. Moreover, TEM analysis revealed that nanoparticles contain high density of planar defects in the form of dislocations. Optical characterization was done using UV-Vis Spectroscopy, for band gap calculations. Further investigation of defects by Photoluminescence spectroscopy revealed highly defected nanoparticles, ultimately, offering possibility in visible range photoresponse of prepared ZnO nanoparticles. Hence, visible light photo-catalysis chamber was designed and developed at SCME to carry out the degradation studies of methylene blue dye. All of the synthesized nanoparticle catalysts exhibited excellent visible light photocatalytic activity ranging from 93.86% up to 99.39% degradation of methylene blue in 50 minutes. This enhanced photocatalytic activity has been attributed to the excessive defects, present in the form of dislocations, instigated via oxygen vacancies and surface hydroxyl group which effectively repress electron-hole recombination by taking care of charge carrier trapping and transferring. Nanoparticle showing highest photocatalytic activity was further tested for degradation of Rhodamine B dye and results concluded 98.85% degradation in an hour. Therefore, described synthesis procedure can be used for commercial scale production of visible active ZnO nanoparticle catalyst with controlled defects offering reproducible luminescence properties, opening possibilities in number applications via simple and cost-effective synthesis route.

Keywords: coprecipitation; ZnO; nanoparticles; methylene blue; rhodamine B; visible light photocatalysis.

Table of Contents

List of Figures

List of Tables

Abbreviations

%	Percentage
$(CH_3COOH)_2Zn.2H_2O$	Zinc acetate dihydrate
$(Zn(NO_3)_2.6H_2O$	zinc nitrate hexahydrate
<	Less than
>	Greater than
≤	Less than and equal to
≥	Greater than and equal to
$^{\bullet}OH$	Hydroxyl radical
°C	Degree centigrade
µM	Micromolar
0D	Zero-dimensional
1D	One-dimensional
2D	Two-dimensional
3D	Three-dimensional
Å	Angstrom (x 10^{-10}m)
Ag	Silver
Al	Aluminum
AMTIR crystal	Amorphous material transmitting Infrared radiation
ATR-FTIR	Attenuated total reflection-Fourier-transform infrared spectroscopy
Au	Gold
C	Carbon
C_2H_5OH	Ethanol
CB	Conduction band
cm^{-1}	Per centimeter
Co	Cobalt
Cr	Chromium
Cu	Copper
CVD	Chemical vapor deposition
CVS	Chemical vapor synthesis
DLE	Deep level emission
DMSO	Dimethyl sulfoxide
DSSC	Dye sensitized solar cell
e^-	Electron
e.g.	For example
E_g	Bandgap Energy
eV	Electron volt
F	Fluorine
Fe	Iron
Fe_2O_3	Iron oxide
g	Gram
h^+	Hole
H_2O_2	Hydrogen peroxide
HCl	Hydrochloric acid

HeCd	Helium Cadmium
HUMO	Highest occupied molecular orbital
i.e.	That is
IR	Infrared
IUPAC	International Union of Pure and Applied Chemistry
LCDs	Liquid crystal displays
LEDs	Light emitting diodes
LUMO	Lowest unoccupied molecular orbital
M	Molar
MB	Methylene blue ($C_{16}H_{18}ClN_3S.xH_2O$)
meV	Million electron volts
mg	Milligram
min	Minute
min^{-1}	Per minute
mL	Milliliter
N	Nitrogen
NaOH	Sodium hydroxide
NBE	Near band edge
nm	Nanometer
NPs	Nanoparticles
O_2	Molecular oxygen
$O_2^{\bullet-}$	Superoxide radical
OCl	Hypochlorite ion
–OH	Hydroxyl group
O_i	Oxygen interstitial
O_{Zn}	Oxygen anti-site
PCA	Photocatalytic activity
Pd	Palladium
Pl	Photoluminescence
Pt	Platinum
PVD	Physical vapor deposition
R^2	Linear correlation coefficient
Rh	Rhodium
RhB	Rhodamine B($C_{28}H_{31}ClN_2O_3$)
rpm	Revolution per minute
S	Sulphur
sec	Seconds
SEM	Scanning Electron Microscope
SrCrO4	Strontium chromate
TEM	Transmission Electron Microscope
TiO2	Titanium dioxide
UV	Ultraviolet
UV-VIS	Ultraviolet-Visible
VB	Valance band
W	Watt
W	Tungsten
XRD	X-ray Diffraction
ZA	Zinc acetate
Zn	Zinc

ZN	Zinc nitrate
ZnO	Zinc Oxide
ZS	Zinc sulphate
α	Absorption coefficient
θ	Angle theta
λ	Lambda

Chapter 1: Introduction

Materials have been center of human attention since the beginning of time and hence the pursuit of better and better materials with enhanced chemical, physical and mechanical properties, has always been rage amongst scientists and researchers. This is where 'nanotechnology', an interdisciplinary field of science, comes into play.

1.1 Nanotechnology

'Nano', a Greek prefix, denotes something extremely small or miniature in size and is one billionth (10^{-9}) of a quantity in terms of measurement [1]. Nanotechnology is the use of nano-sized materials to fabricate devices for various practical applications. Hence, nanotechnology is all about material engineering at molecular or even atomic level to gain control over material properties which are governed by the laws of quantum physics.

Nature offers numerous examples of nanoscience e.g. Abalone, from phylum Mollusca creates strong nanoscale shell of calcium carbonate around itself [2], the strength and durability of cotton is due to cellulose fibers nanoscale arrangement and it's the hierarchical nanostructures in toes of Gecko which help it in sticking to the walls [1]. Furthermore, the history dictates that Chinese and Romans have known to color their ceramic porcelains and glass artifacts [3] but it was Michael Faraday who is credited for birth of nanoscience, in 1857, because of his explanation regarding color variations of gold nanoparticles as a result of change in size of nanoparticles . However, it is the famous talk "There is Plenty of Room at the Bottom", delivered by Richard Feynman in 1959, that really resonates with todays 'Nano Era', although it was not acknowledged as nanotechnology at that time [2].

1.1.1 Nanomaterials

A material is classified as a nanomaterial if at least one of its dimensions is in the nanometric range i.e. size less < 100nm, and on this basis they are classified into following categories [4]:

- Zero dimensional (0D) structures: all the three dimensions in nanometer range, e.g. nanoparticles and quantum dots.

- One dimensional (1D) structures: two dimensions are in nanometer range, e.g. nano- rods, wires, needles, spikes, rings, helix, springs, combs, belts, ribbons and tubes. It's the largest group of nanostructures.
- Two dimensional (2D) structures: one dimension in nanometer range, e.g. nanoplate/nanosheet and nanopellets
- Three dimensional (3D) or bulk structures: all dimensions are greater than nanometer range, e.g. flowers, dandelion, snowflakes and coniferous urchin-like, etc. These can result from cluster or agglomeration of 0D, 1D or 2D nanostructures.

1.1.2 Unique Properties

Some of the unique properties offered by nanomaterials are:

- Electromagnetic forces dominate while the gravitational forces become negligible.
- They have high kinetic energy despite small mass therefore wave-particle duality allows tunneling in nanomaterials unseen in case of bulk materials.
- Atoms and electrons are confined due to small size of nanomaterials rather than moving freely in bulk materials.
- Energy quantization occur because electrons can exist in discrete energy levels and exciton can exist in all three dimensions e.g. in quantum dots.
- High surface to volume ratio, is one of the most beneficial aspect of nanomaterials.

1.1.3 Synthesis Techniques

Synthesis methods for nanomaterials involve two basic approaches which are mentioned below, and the various techniques classified and summed up by Salaheldeen Elnashaie [5] and are shown in fig.1.1.1:

1.1.3.1 Bottom Up

In bottom up approach the small components up to atomic size arrange themselves in specific patterns to form nanostructures. If the process parameters are well controlled this synthesis method gives very fine nanostructures, individual NPs and nano shells etc. with fine size distribution. However, scaling up is difficult in this approach.

1.1.3.2 Top Down

In top down synthesis approach large components are broken into smaller pieces until nanometer scale. It is helpful in creating bulk nanostructures unlike individual NPs from bottom up approach. Scaling up is easy in top down synthesis approach.

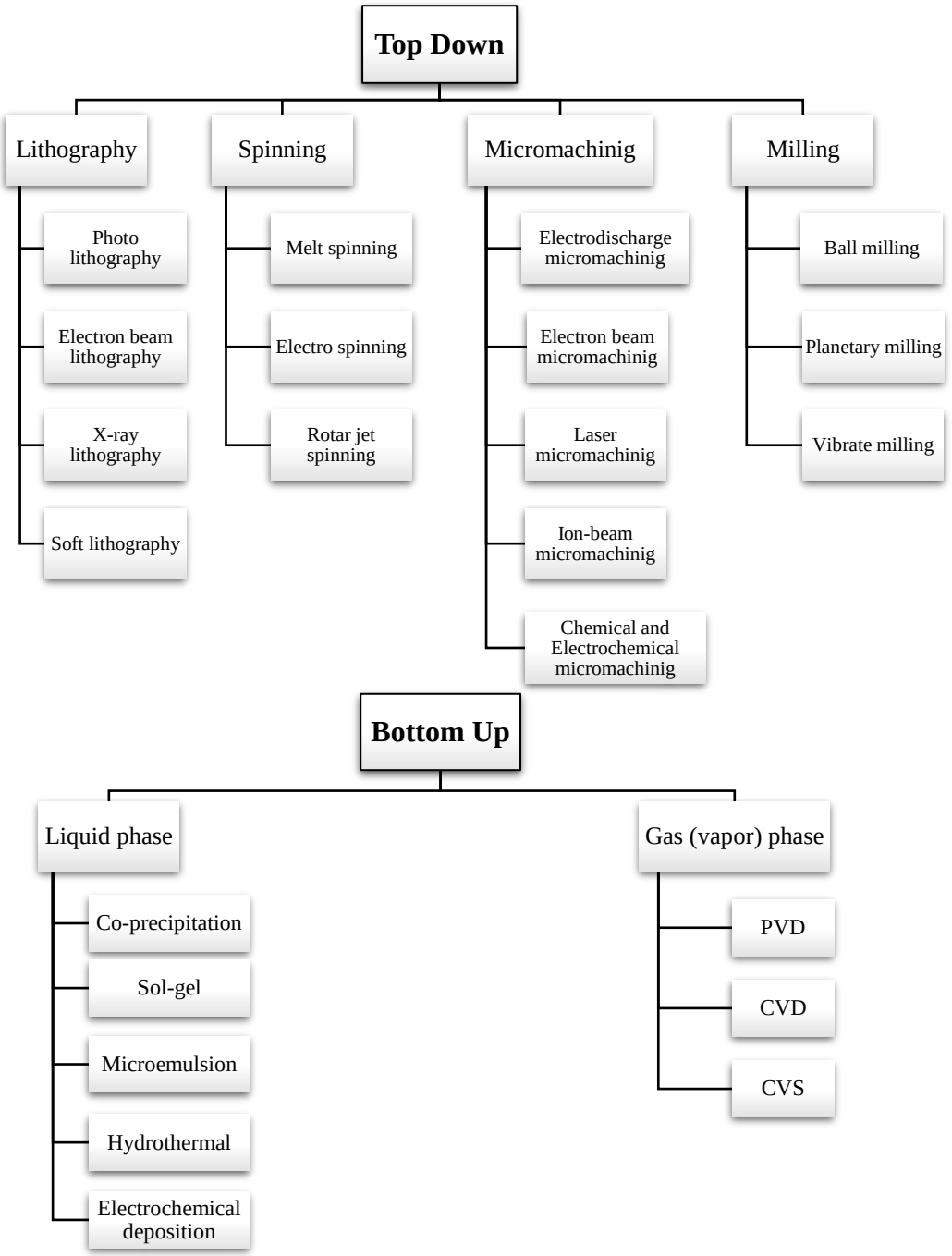

Fig. 1.1.1 Classification of various synthesis techniques used for synthesis of nanomaterials.

1.1.4 Applications of Nanomaterials

Nanomaterials have wide range of applications in every field of science. Some of the which are:

1.1.4.1 Electronic and Opto-electronic Devices

Nanoscience has revolutionized the opto-electronic industry. In last few decades there has been dramatic decrease in the size of electronics devices with enhanced efficiency. Nanoscience is also responsible for making smaller transistors using various semiconductors thus making possible lab on chip strategies. Flexible electronic devices are also a gift of nanotechnology. Various Opto-electronic devices such as LEDs, LCDs, photodetectors, and solar cells use nanotechnology for improvement in performance. For instance, computer screens, DVD players, mobile phones, automobile illuminators and digital cameras make use of thin film transistor technology.

1.1.4.2 Biomedical Application

Nanoscience has brought revolution in biomedical sciences. Several new nanorobotics devices are formed which not only help in in-vivo diagnosis but also help in transfer of drugs within the body. Vivo imaging with minimum miniaturization is now possible because of nanoscience. These nano devices helps in opening up of clogged arteries, removing stones from various body parts and perform several other functions. In addition to wound dressings, nanomaterials have now been widely used in cancer treatment, artificial bone grafting, and bone and tissue regeneration. These materials have helped in cutting down complex surgical procedures proving not only efficient but cost-effective as well. Nanomaterials are also used in artificial biosensors in which metal NPs are used to modify the surface of electrodes. Enzyme modified biosensors offering better compatibility with living systems are now available for use in bio-electro chemistry e.g. carbon paste electrodes for the detection of glucose level. Nanobots or nano-robots are recent advancement in drug delivery systems thanks to nanotechnology.

1.1.4.3 Renewable Energy

Nanoscience has provided various clean methods for energy production. Solar cells, photovoltaic devices and DSSC use nanomaterials for maximum absorption and conversion of solar energy into chemical and mechanical energy which is further used in power sector as well as commercial sector. Highly efficient, less hazardous, small

batteries have also developed. Green fuels for automobiles such as hydrogen can be produced using photolysis and artificial photosynthesis process in lab by environment friendly methods thanks to nanoscience.

1.1.4.4 Cosmetics and Textile Industry

Cosmetics and textiles industries are using NPs widely. NPs are now being used in sun blocks, face creams and shampoos. In textile industry nanomaterials are used for the production of strong fibers, flexible clothes with long life, self-cleaning clothes and in dying.

1.1.4.5 Environmental Applications

- Catalysis: Nanotechnology's most lucrative application perhaps lies in catalysis because nanomaterials offer extremely large surface-to-volume ratio making them more active catalysts. Hence, removal of the hazardous chemicals released from industries using nanomaterials has been used widely for purification of surface and ground water, soil and hazardous industrial waste.
- Consumer Products: They also help in the creation of self-cleaning surfaces like walls, clothes etc. which reduce the need of cleaning agents thus prevent environment from pollution.
- Food: Environment friendly energy sources with high efficiency, fertilizers and automobiles has been developed which make environment less pollutant and possess high efficiency. Nanomaterials are been widely used in food packaging which are made up of biodegradable materials. These packings not only increase the shelf life of food with no change in taste but also degrade into biological entities thus protecting environment from polymer pollution.

1.2 Photocatalysis

The word Photocatalysis is derived from Greek language in which "phos" signifies light and "katalyo" means to break apart or decompose. After exhausting debate on definition of photocatalysis, the International Union of Pure and Applied Chemistry (IUPAC), delivered a verdict that the term Photocatalysis stands for the reactions which are carried out in the presence of a semiconductor and light [6]. Hence, Photocatalysis involves reactions which make use of a photocatalyst, a substance particularly a semiconductor which absorbs light for its activation, to derive forward a chemical reaction modifying its rate, without being involved itself. In general, the

basic principle of photocatalysis is semiconductor activation by irradiating it with light source of appropriate wavelength to eradicate various pollutants (e.g., alkanes, alkenes, phenols, aromatics, pesticides) and complete mineralization of the organic compounds.

Reactant's physical state classifies the photocatalytic reactions into following two categories:

1.2.1 Homogeneous Photocatalysis

It's the reaction in which both the photocatalyst and the reactant exist in same phase, i.e. solid, liquid or gas. Examples include natural pigments, organic substances, dyes etc.

1.2.2 Heterogenous Photocatalysis

Reaction in which the photocatalyst and reactant exist in different phases, it is called as heterogeneous photocatalysis. Solid photocatalyst (e.g. transition metal chalcogenides) interaction with either a liquid or a gas is a typical example of heterogeneous photocatalysis.

1.2.3 Mechanism

A photocatalyst absorbs photons upon light irradiation of suitable wavelength, i.e. energy equal to or higher than the bandgap of a photocatalyst, this marks the beginning of photocatalytic reactions. The absorption of photons initiates charge separation by promoting valence band (VB) electrons (e^-) to the conduction band (CB) creating holes (h^+) in its wake. This is also referred as 'photo-excitation state'. These newly formed e^- and h^+ can either recombine releasing heat or they can migrate to the surface of the particle where they can react with adsorbed molecules. Electrons in the conduction band have a potential to reduce a substance e.g. e^- react with O_2 reducing it to superoxide anion radical $O_2^{\bullet -}$ whereas, holes in the valence band can be exploited for oxidation e.g. h^+ reacts with –OH or water and oxidizes them to $^\bullet$OH radicals, or it can cause direct oxidation of an organic molecule to R^+. The photocatalytic activity hinges on the catalyst's ability to produce electron–hole pair, as there is good enough probability that the generated electrons may lose the energy and get back to their valence band positions annihilating the holes which were created. Hence the relative position of the conduction and valence bands in a semiconductor photocatalyst and substrate's redox levels are pivotal in defining the fate of generated e^-–h^+ pairs [7].

1.2.3.1 Photocatalytic Degradation Reactions

Three basic photocatalytic degradation processes given below are shown in Fig.1.2.1 [6]:

1. Oxidation
2. Electron injection.
3. Redox reactions.

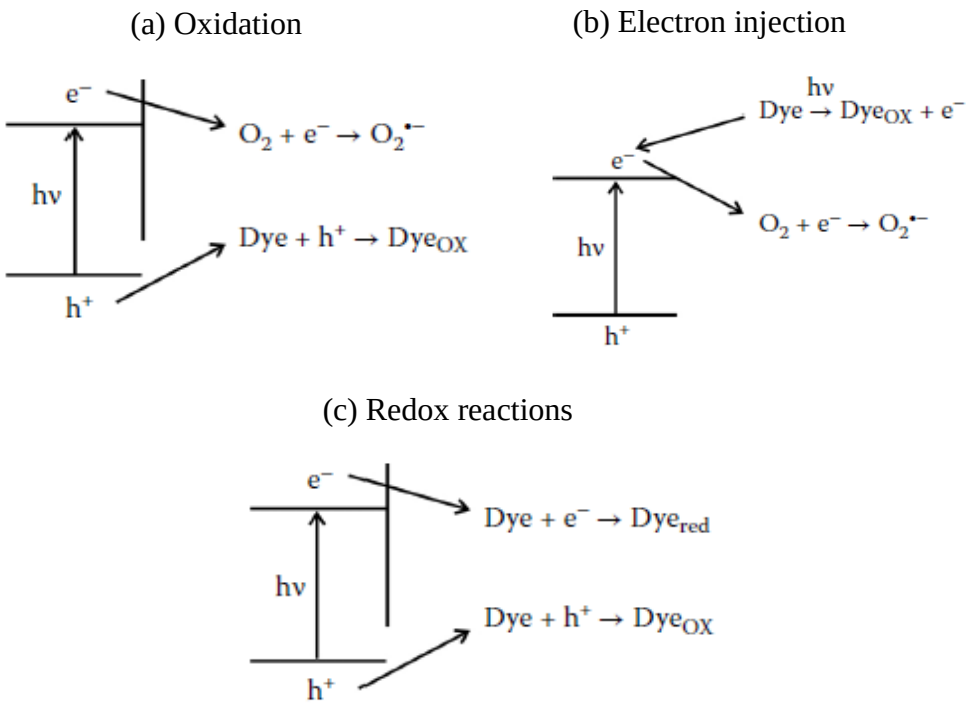

Fig. 1.2.1 Photocatalytic degradation processes.

The four possible combinations of semiconductor relative bands positions and substrate redox levels are as follows:

1. Substrate's reduction takes place if it's redox level is lower than the CB of the semiconductor.
2. Substrate's oxidation occurs if it's redox level is higher than the semiconductor's VB.
3. If substrate's redox level lies in between semiconductor's CB and VB, then both oxidation and reduction takes place
4. There is no reaction if substrate's redox level is higher than the CB and lower than the VB of the semiconductor.

1.2.3.2 Reactive Oxygen Species

The major reactive oxygen species involved in photocatalysis are:

- Molecules like hydrogen peroxide H_2O_2
- Ions like hypochlorite ion (OCl^-)
- Radicals like the hydroxyl radicals ($^{\bullet}OH$)
- Superoxide anion ($O_2^{\bullet-}$), which act as both an ion as well as a radical.

In the aforementioned species, the hydroxyl radical is the most reactive and potent oxidizing agent (relative oxidation power of 2.06eV), promptly removing electrons from any molecule present in vicinity yielding a free radical and initiating chain reactions.

1.2.4 Semiconductor Photocatalysts

The fact that upon exposure to light source of sufficient energy ($\geq E_g$, band gap energy), a semiconductor can conductor electricity at room temperature makes it one of the compelling contenders amongst photocatalysts. Generally, the energy gap between conduction band (LUMO) and valence band (HOMO), of a semiconductor ranges from 1.5 to 3.0 eV. Binary semiconductors are the most prevalent photocatalysts and examples includes ZnO, TiO_2, Fe_2O_3 etc. Examples of ternary semiconductor photocatalysts are $PbCrO_4$, $SrZrO_3$, $CuInSe_2$ etc. whereas, quaternary semiconductor like $Cu_2ZnSnSe_4$, Bi_2AlVO_7, $FeZn_2Cu_3O_{6.5}$ etc. have been scarcely used as photocatalyst.

1.2.4.1 Modifications

Scientist and researchers have exploited various strategies to enhance photocatalytic activity of semiconductors by altering their physical parameters such as morphology, size, bandgap and surface modification etc. Some of the most commonly used techniques are:

- Doping and Co-doping:

  The intentional addition of extrinsic semiconductor impurities in a substance is termed as doping which can either be p-type (cationic, e.g. Cu, Fe, Al, Co, etc.) or n-type (anionic, e.g. C, F, N, S, etc.) depending upon the variety of dopant added. The main idea of doping is to enhance photoresponse of a material by creating new energy levels. Co-doping is addition of more than one dopant and

examples are Cu-Al co-doped ZnO, W-C co-doped TiO_2 and Cr-N co-doped ZnO.

- Composite:

  Semiconductor coupling of material having different bandgaps can result in CB electron transfer from smaller bandgap material to higher bandgap material enabling photocatalytic activity e.g. NiS/$Zn_xCd_{1-x}S$/reduced graphene.

- Metallization:

  Noble metals such as Pt, Au, Pd, Ag, Rh, etc. improve photocatalytic activity by suppressing e^-–h^+ recombination.

- Dye Sensitization:

  In this process, upon exposure to light source ($\lambda \geq 420$nm), dye molecule gets excited by releasing electron to the semiconductor CB hence initiating the photocatalytic activity e.g. Methylene Blue (MB).

Problem Statement

Despite the well-known fact that water covers 70% of the earth surface, all of it is not fit for human consumption and other purposes. Industrial revolutionization, didn't only result in mankind's development and betterment but also came with the devastating consequences in the form of hazardous wastewater discharge. It consists of heavy metals and toxic organic and inorganic compounds like phenols, dyes, detergents, insecticides, pesticides, surfactants, fertilizers and several other chemical products. This wastewater is dumped into rivers and canals without any treatment hence a major culprit in water pollution, which not only affects the human beings but animals and plants as well.

Therefore, state-of-the-art measures are needed for purification and recycling of wastewater by various industries. Photocatalysis, as of late has come up as a promising technique for the treatment of robust pollutants, for it is simple yet cost-effective. It works by exploiting the photoresponse of a material (generally a semiconductor) for degradation of dyes used by various textile industries for coloring.

Objectives

Following aims and objectives have laid foundation for this research:

- Synthesis of zinc oxide nanoparticles via coprecipitation technique.
- Investigations into effect of synthesis parameter, namely salt precursor and synthesis temperature, on physical, chemical and optical properties of prepared nanoparticles.
- Visible light degradation and its mechanism study for methylene blue and rhodamine B dyes via prepared ZnO nanoparticle catalysts.

Chapter 2: Literature Review

2.1 Zinc Oxide

2.1.1 Crystal Structure

Zin oxide (ZnO) is a II–VI compound semiconductor with ionicity residing borderline between the covalent and ionic semiconductors. It can exist in three crystal structures namely wurtzite (B4), zinc blende (B3), and rocksalt (B1) (or Rochelle salt), shown in Fig 2.1.1, with wurtzite being the most thermodynamically stable phase under ambient conditions. Rocksalt can be obtained at high pressures whereas zinc blende shows stability only when grown on cubic substrates.

The wurtzite structure has a hexagonal unit cell with two lattice parameters a and c in the ratio of c/a = $\sqrt{8/3}$ = 1.633 (in an ideal wurtzite structure) and belongs to the space group C_{6v}^4 in the Schoenflies notation and $P6_3mc$ in the Hermann–Mauguin notation. The structure is composed of two interpenetrating hexagonal close packed (hcp) sublattices, each of which consists of one type of atom displaced with respect to each other along the threefold c-axis by the amount of u = 3/8 = 0.375 (in an ideal wurtzite structure) in fractional coordinates. The internal parameter u is defined as the length of the bond parallel to the c-axis (anion–cation bond length or the nearest-neighbor distance) divided by the c lattice parameter. The basal plane lattice parameter (the edge

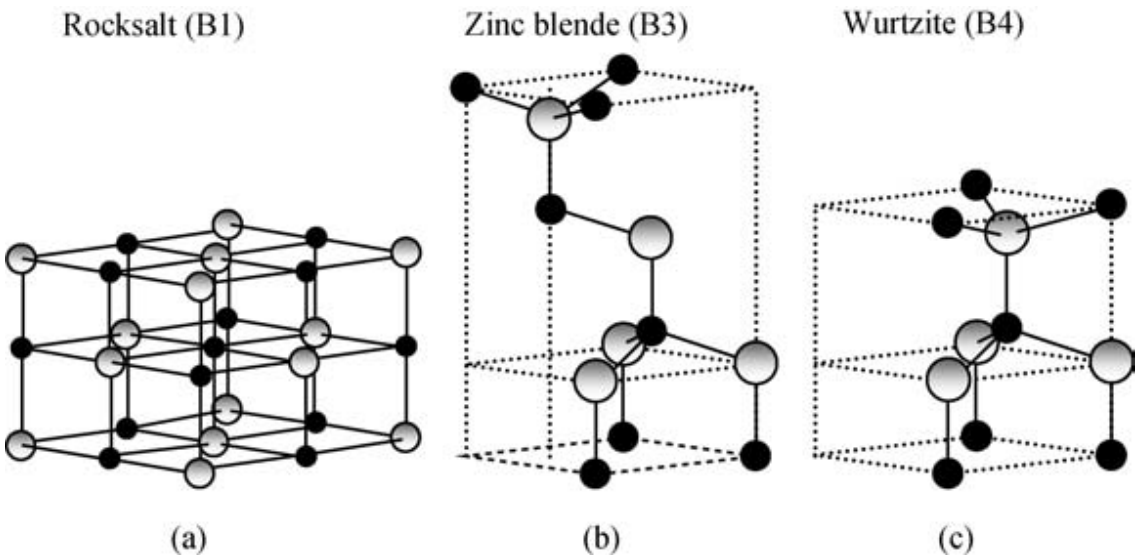

Fig. 2.1.1 Stick-and-ball representation crystal structure for **(a)** cubic rocksalt (B1); **(b)** cubic zinc blende (B3); and **(c)** hexagonal wurtzite (B4). B1, B3 and B4 denotes the Strukturbericht designations for the three phases. Shaded gray and black spheres represent Zn and O atoms, respectively.

length of the basal plane hexagon) is universally depicted by a; the axial lattice parameter (unit cell height), perpendicular to the basal plane, is universally described by c. Each sublattice includes four atoms per unit cell, and every atom of one kind (group II atom) is surrounded by four atoms of the other kind (group VI), or vice versa, which are coordinated at the edges of a tetrahedron. The crystallographic vectors of wurtzite are $\vec{a} = a(\frac{1}{2}, \frac{\sqrt{3}}{2}, 0)$, $\vec{b} = b(\frac{1}{2}, \frac{-\sqrt{3}}{2}, 0)$ and $\vec{c} = c(0,0,c/a)$. In Cartesian coordinates, the basis atoms are (0, 0, 0), (0, 0, uc), $a(\frac{1}{2}, \frac{\sqrt{3}}{2}, \frac{c}{2a})$ and $a(\frac{1}{2}, \frac{\sqrt{3}}{6}, \frac{[u+\frac{1}{2}]c}{a})$ [8, 9].

The structure of ZnO can be simply described as a number of alternating planes composed of tetrahedrally coordinated $O_2^-$and Zn^{2+} ions, stacked alternately along the c-axis. The tetrahedral coordination in ZnO results in non-central symmetric structure and consequently piezoelectricity and pyroelectricity. Another important characteristic of ZnO is polar surfaces. The most common polar surface is the basal plane. The oppositely charged ions produce positively charged Zn–(0001) and negatively charged O–$(000\bar{1})$ surfaces, resulting in a normal dipole moment and spontaneous polarization along the c-axis as well as a divergence in surface energy. To maintain a stable structure, the polar surfaces generally have facets or exhibit massive surface reconstructions, but ZnO ±(0001) are exceptions: they are atomically flat, stable and without reconstruction. The other two most commonly observed facets for ZnO are $\{2\bar{1}\bar{1}0\}$ and $\{01\bar{1}0\}$, which are non-polar surfaces and have lower energy than the facets. Structurally, ZnO has three types of fast growth directions. Together with the polar surfaces due to atomic terminations, ZnO exhibits a wide range of novel structures that can be grown by tuning the growth rates along these directions. One of the most profound factors determining the morphology involves the relative surface activities of various growth facets under given conditions. Macroscopically, a crystal has different kinetic parameters for different crystal planes, which are emphasized under controlled growth conditions. Thus, after an initial period of nucleation and incubation, a crystallite will commonly develop into a three-dimensional object with well-defined, low index crystallographic faces [10, 11].

2.1.2 Basic Properties

ZnO in a unique material for it can be grown into rich variety of morphologies as well as exhibits wide range of useful properties, some of which are [9]:

2.1.2.1 Bandgap

The direct band gap of ZnO is a function of temperature, and is 3.37eV at room temperature whereas, it drops to 3.44eV at low temperatures. ZnO exhibits a direct band gap. However, certain approaches have been used by scientists and researchers for extending the bandgap suitable for numerous applications.

2.1.2.2 Exciton binding energy

Exciton binding energy of ZnO is reported to be approximately 60 meV indicating that ZnO devices remain stable even when giving emissions at room temperature. This is because the oscillator strength in ZnO is found to be much larger than the strength contributed by the electron-hole pair generation in direct band gap structures. Thus, the high exciton binding energy makes ZnO an attractive material for various optical devices.

2.1.2.3 Piezoelectricity

Some materials have crystal structures with a pair of charges that can cancel each other in equilibrium positions. When distortion occurs, the charges cease to cancel each other out thus developing a minor voltage. This can be used to generate a current which can be amplified to give readings. The principle is known as piezoelectricity and such materials are called piezoelectric materials. The phenomenon is reversible i.e. both mechanical stress and electrical energy can be applied to generate the other. Such materials have found their use in sensors, transducers and actuators. Asymmetrical in nature, ZnO tends to portray a high piezoelectric and pyroelectric constant.

2.1.2.4 Luminescence

ZnO displays strong luminescence in the UV–Visible of the electromagnetic spectrum, making it apt material for phosphor related applications. Although the origin of luminescence centers has no consensus amongst scientists and researchers as of yet and the involved mechanics are not clear, but ZnO still finds uses in photocatalysis because of these defect related emissions.

2.1.2.5 Surface sensitivity

ZnO is sensitive to the presence of different species of gases within its environment and its conductivity is therefore affected by the concentration of the gases present. Recent experimental data shows that upon exposure to air surface charge accumulation

in the form of electrons, disappears which can enable sensing action e.g. freshness of drinks and foo can be monitored by sensing trimethylamine odor.

2.1.2.6 Nonlinear resistance

Grain boundaries and related microscopic mechanisms are responsible for nonlinear resistance in ZnO which still needs further clarification as the mechanism is far from fully understood. Nonetheless it imparts highly nonohmic current–voltage characteristics in ZnO allowing use in devices such as varistors.

2.1.2.7 Nonlinear optical coefficients

A linear relationship between polarization density and the electric field defines the linear optics. The relationship is linear for small values of permittivity and deviates as the permittivity value surpasses a certain limit showing nonlinear behavior. ZnO crystal lacks inversion symmetry therefore shows strong second- and third-order nonlinear optical behavior attractive for integrated non-linear optical devices.

2.1.2.8 Thermal conductivity

The thermal conductivity of ZnO is very high therefore it can be used as an additive to increase the thermal stability e.g. in rubber tyres. Furthermore, it makes ZnO substrates appealing for homoepitaxial as well as heteroepitaxial growth. High thermal conductivity pertains to efficient heat removal throughout device operation.

2.1.2.9 Amenability to wet chemical etching

ZnO shows exemplary response to various low temperature etching environments either basic, acidic or other solution mixtures. Hence, allows control in designing and processing of various optoelectronic devices.

2.1.2.10 Radiation hardness

It is a property which makes a device resistant to ionizing radiation and associated damage and has applications in outer space devices where high radiation values are needed. ZnO possesses extremely high radiation hardness values much more so than GaN.

2.2 Coprecipitation Synthesis of ZnO NPs

Coprecipitation is one of the most used methods amongst nanomaterials synthesis [12], for it is simple and cost-effective and therefore, this approach has been the focus for synthesis of ZnO nanoparticles of in this research. An insoluble solid that forms during

a reaction is called a precipitate and reaction forming precipitates is termed as precipitation reaction. The basic elements of precipitation process are shown in Fig 2.2.1. A reaction can either result in direct metal oxide formation, or in most of the cases, it produces a precursor which is then subjected to post-precipitation processes such as filtration, washing, drying and calcination [13].

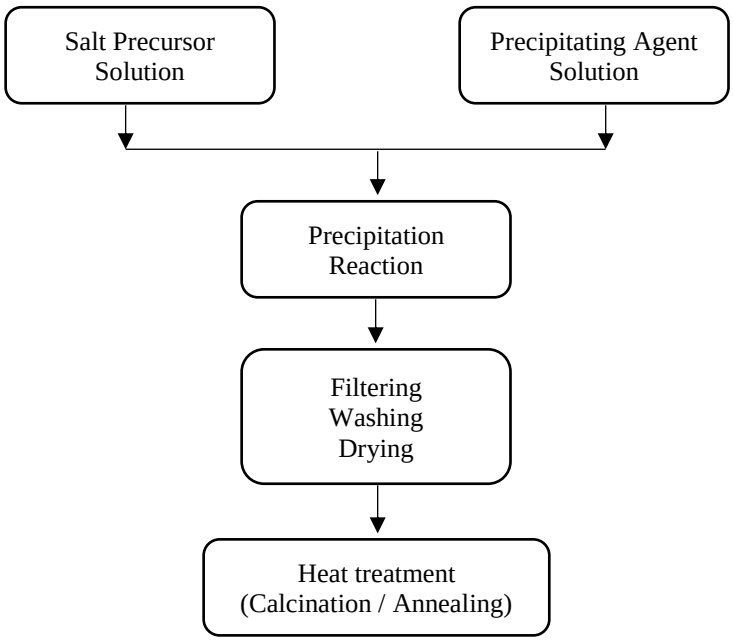

Fig. 2.2.1 Schematics for a precipitation synthesis.

Nanoparticles formation does not result from mere precipitation rather simultaneous occurrence of nucleation, growth, coarsening, and/or agglomeration dictates the outcome. Nucleation is the most critical step in which large number of small crystallites are formed simultaneously, from a supersaturated solution followed by growth into stable particles. The growth is affected by processes such as Ostwald ripening, agglomeration etc. Ostwald ripening is the growth of larger particles at the expense of smaller ones, and occurs at low temperatures whereas, agglomeration is formation of particle clusters as a result of chemical bonds and physical attractive forces at interfaces. The smaller the particle is, the higher the chances of agglomeration because of greater bonding forces [14]. Hence, for nano sized particles the nucleation rate should be higher than the growth rate. In order to attain monodisperse nanoparticles, stabilizers are needed to prevent agglomeration, and the two basic approaches are [15]:

1. Addition of capping agents, i.e. surfactants, polymers or other surface bound organic species to introduce steric repulsion between the particles.

2. Chemisorption of charged species (H^+ or OH^-) on the particle surface to introduce electrostatic repulsion between particle.

Post synthesis thermal treatments e.g. calcination or annealing results in inevitable agglomeration thus increasing particle size and compromising size distribution, therefore, monodisperse nanoparticles cannot be formed.

Zinc oxide is one of the promising materials, not only in terms of application in various fields but it also exhibits rich assortments of nanostructures which are easy to synthesize via chemical route. There exists vast amount of literature, regarding variation and modifications in synthesis parameter of coprecipitation technique for ZnO nanoparticles, in order to fine tuning its properties for use in desired application. The upcoming section discusses some of these synthesis parameters as well as the existing literature relevant to ZnO nanoparticles.

2.2.1 Factors Affecting Coprecipitation

Following are essential parameters, with influential role is in defining the fate of nanoparticles as an outcome in coprecipitation synthesis:

2.2.1.1 Rate of precipitation and method of addition

Slow precipitation yields large but well crystallized nanoparticles and can be achieved by gradual addition of dilute precipitating solution. This is because fewer nuclei are formed and hence they have sufficient time to grow into well-defined crystals. Rodriguez has explained controlled precipitation in his article [16] by controlling the release of cation through titration. Moezzi [17] studied method of combing reactants buy experimenting four approaches, drop by drop addition of precipitating agent, NaOH into salt solution and its vice versa and then single addition of whole precipitating agent into salt solution and vice versa. The study concluded that smaller nanoparticles are formed if NaOH in added into salt solution.

2.2.1.2 Reactants Stoichiometry and pH

Larger crystals are formed if the concentration of ions is low in a solution (but adequate enough for precipitation). Since change in ion concentration changes the pH of aqueous solution as well therefore it's imperative to study the effect from both aspects pH as well ion concentration. This effect of change in salt solution concentration has been studied by Moezzi [17] along with method for combining reactants and reaction temperature. According to his study different precipitating product, zinc oxide or zinc

hydroxide is formed by change in concentration of reactants. Koutu varied concentration of NaOH in his experiments [18] and concluded that particle size increases with increase in NaOH concentration as well as the change affects the optical properties of nanoparticle. Similar conclusions were drawn by Swaroop [19] in study based on effect of pH. However, a different conclusion was presented by Chithra [20] claiming that particle size increases with the increase in solution pH and brings variations to the UV emission in Pl spectra without any significant change in visible emission.

2.2.1.3 Temperature

An optimum temperature condition has to be balanced in order to get smaller nanoparticles. Either a very high temperature or very low temperature is undesirable because nucleation is slow at high temperature while growth increases and secondly at low temperature solubility of most solids decreases which reduces the precipitate yield. Manzoor in his two different articles on ZnO nanoparticles studied the effect of temperature along with other parameters as well. The findings conclude that increase in temperature increases the particle size with improved crystallinity [21, 22]. Similar conclusion was drawn in [23] with the addition that particle morphology also changes with variation in synthesis temperature. The temperature related thermodynamic analysis has been investigated in detail by Richardson and Lange and the readers are directed to their article [24] for better understanding of related concepts.

2.2.1.4 Salt Precursor

Role of salt precursor solution is really important as different anions involved bring in different chemistry in synthesis mechanism which affects morphology and size of nanoparticle. ZnO synthesis via different salt precursors involving different anions i.e. chloride, nitrate, sulfate, and acetate has been studies by Srikanth [25]. According to the results zinc chloride salt yielded plate-like morphology, while $Zn(NO_3)_2$ and $ZnSO_4$, produce spherical nanoparticles and irregular agglomerated particles were produced via $Zn(CH3COO)_2 \cdot 2H_2O$. Furthermore, zinc nitrate yielded the smallest nanoparticles of 32nm size in comparison to other zinc salts. It is also concluded in article [26] that nitrate precursor yielded the smallest nanoparticles amongst zinc nitrate, zinc chloride and zinc acetate salts. Pudukudya and Yaakob [27] synthesized novel nanostructures by using acetate, chloride, nitrate and sulphate salt precursors. They obtained highly porous micro disc like ZnO morphology via sulphate and nitrate

counter ions by using zinc sulphate and zinc nitrate respectively. Other studies regarding change in salt precursor in obtaining ZnO includes [28, 29].

2.2.1.5 Solvent

The amount of solute, soluble in a solvent depends upon the nature of solvent as well because of polarity. Hence, in coprecipitation addition of alcohols is often reported which affects the dielectric constant of the solvent as well. Kumar and his group [30] prepared ZnO nanoparticles via coprecipitation method using water, methanol, ethanol and DMSO medium as solvent. The result shows variation in size and optical properties in nanoparticles as a result of medium change.

2.2.1.6 Degree of supersaturation

The physical property of a resulting precipitate is dependent upon degree of supersaturation. Higher degree of supersaturation causes spontaneous nucleation allowing more aggregation with faster crystal growth. Whereas, at low supersaturation few nuclei are formed with slow growth rate allowing the crystal to grow in perfection, and this happens when low concentration of ions is used for required supersaturation limit.

2.2.1.7 Stirring

Stirring keeps solution thoroughly mixed by providing motion to the reactants hence avoiding any buildup of localized ions' concentration and promoting recrystallization.

2.2.1.8 Growth Time

When a precipitate is allowed to grow over time i.e. when expose to heating, the Ostwald ripening allows growth of larger crystals at the expense of smaller crystals. This is because smaller particles are more soluble than large particles reason being their large surface area and hence, they dissolve. The process causes reduction in available surface area for adsorption of impurity ion hence allows the crystal growth to fit desired lattice. This effect has been studied [31] and the results are surprising since its concluded that particle size decreases with increase in heating time. The heating time was varied from 3hr to 5hrs and the resulting crystallite size were 66nm, 27nm and 12nm for 3hrs, 4hrs and 5hr heating time respectively. However, the TEM result indicated 11-20nm particle size for 5hr heating time showing inconsistency in the results.

2.2.2 Post-synthesis Heat Treatment

Synthesis of nanomaterials is often followed by heat treatment such as calcination, annealing or sintering in various environments and operating condition. This step often leads to increase in size particle size so at times researchers prefer to skip it. On the other hand, heat treatment of nanomaterials remarkably affects their optical properties Hence, it's an important step, nonetheless.

Sugapriya [32] in his experiments studied the effect of annealing on nanoparticles at various temperatures of 400°C, 500°C and 600°C for one hour in a muffle furnace. The results concluded that the particle size increases with the increase in heat treatment temperature. In addition, it was observed that the absorption edge shifts to the longer wavelengths due to thin increase in size.

Kumar and Sahare annealed the prepared ZnO nanoparticles at different temperatures of 200°C, 400°C, 600°C and 800°C for 5 h in air [33]. Their results describe that heat treatment not only affects the size of nanoparticles, it also changes the morphology from spherical to a random shape at high temperature annealing. Furthermore, a red-shift was observed in the characteristic absorption peak of ZnO, with the annealing temperature, due to the decrease in the band gap. Pl studies showed that annealing affects both the UV and visible region emission in ZnO due to the removal or incorporation of defects in ZnO.

The ZnO nanocones were synthesized by Kavitha and his group [34], which were further subjected to calcination at 550°C in air. Their results revealed that the absorption edge shifts to a higher wavelength after calcination indicating a smaller bandgap for calcined ZnO due to the formation of sub-levels inside bandgap by the defects. The Pl analysis exhibited quenching of green emission with improvement in blue emission as a result of calcination and both these emissions were associated to the oxygen and zinc vacancies respectively, by the authors.

Raoufi [35] also studied the effect of annealed the synthesized ZnO nanoparticles in the muffle furnace at temperature ranging from 250°C to 550°C for 4 h.

ZnO nanostructures prepared by Raji and Gopchandran were heat treated in a muffle furnace from 300°C to 900°C at 5°C min^{-1} for 120 minutes [36]. The study concluded that annealing temperature alter the position of visible emission band from orange to

red and then to green luminescence region and this shift in the visible emission band is attributed to change in the local environment of the defect centers.

2.2.3 Defects and Luminesce in ZnO

The intrinsic 'native' defect related emission in ZnO is usually characterized by room temperature PL spectrum which commonly displays near-band-edge (NBE) ultra-violet (UV) emission and a broad band visible emission related to the deep levels, called DLE which extends from just above 400 nm up to 750 nm. The broadness of the band is representative of superposition of many different deep levels giving of emission at the same time. Different DLE defects have different formation energy and contribution to the conductivity in ZnO and researchers and scientists have labelled them to various different origin with no consensus as of yet. The broadness of the DLE band suggests that it emanates possibly from a combination of many different emissions.

The deep level in ZnO are oxygen vacancy (V_o), zinc vacancy (V_{Zn}), oxygen interstitial (O_i), zinc interstitial (Zn_i), oxygen anti-site (O_{Zn}), and zinc anti-site (Zn_o), additionally there can exists native defect clusters, formed by the combination of two point defects or one point defect and one extrinsic element, e.g., a V_oZn_i cluster formed by zinc interstitial and oxygen vacancy. These native point defects often directly or indirectly control doping, compensation, minority carrier lifetime and luminescence efficiency in semiconductors. In addition, these are often held responsible for inadvertent n-type conductivity in ZnO which pertains to the difficulty in obtaining stable p-type doping. All these point defects can exist in different charged or neutral states and can form the complexes with other native defects or extrinsic species. Hence the large number of luminescence line with varying energies exhibited by ZnO is because of different deep levels invoked at different positions in the bandgap and is the reason for emitting all of the visible colors in different ZnO samples. Some of the literature regarding various defect related emission includes the following research articles [37-52].

2.3 Visible light Photocatalytic Activity of ZnO

The three regions of electromagnetic spectrum which are of interest in photocatalysis are shown in Fig.2.3.1. Various light sources are used according to photocatalysis in desired region for of electromagnetic spectrum, such as xenon arc and H_2, D_2 lamps for ultraviolet; and halogen and tungsten lamps for visible region. Potential photocatalysis in IR region has been recently establish which was not really popular for photocatalysis beforehand [53].

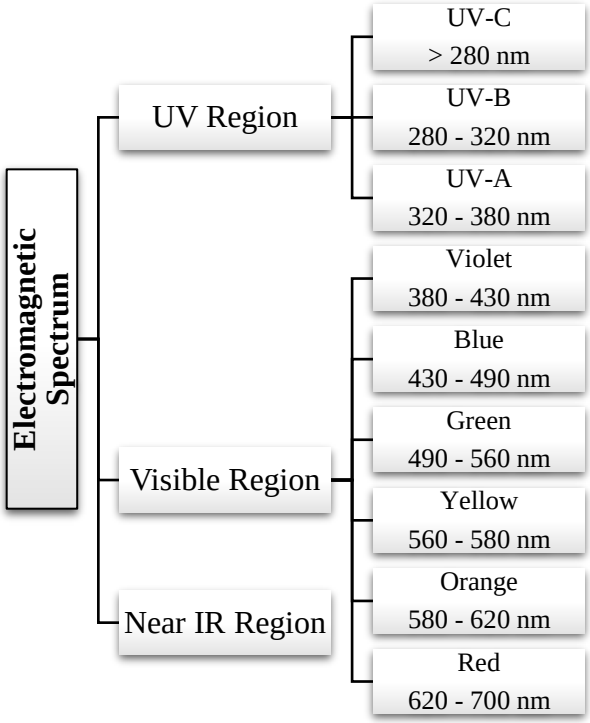

Fig. 2.3.1 Regions of electromagnetic spectrum classified according to wavelength.

Water is a fundamental necessity for existence of all living beings. Water covers 71% of earth's surface but only 2.5% of it is fresh water and fit for consumption. Estimations predict that 50% of people will run out of clean water by 2025 [54]. This entire scenario is further aggravated by industrial discharge dumped into rivers and canals which are natural water reservoirs. The toxic organic, inorganic and microbial contaminants present in these effluents impart major health risks to not only humans but to aquatic and biotic life as well. A fairly large percentage of this wastewater discharge comprises of dyes used by various industries and factories for imparting color to textiles, food items and cosmetics etc. Hence, removal of these toxic and carcinogenic dyes along with other organic contaminants is need of the hour. Hence, industrialists and researchers are in constant pursuit of eco-friendly methods for destruction and degradation of these pollutants.

The solar spectrum comprises of about 3–5% UV ($\lambda < 400$ nm) and about 47% visible light ($400 > \lambda < 700$ nm) in terms of energy, and theoretically, the earth receives about 89,300 TW of solar insolation [55]. This humongous and constant energy source is the reason why photocatalytic degradation of effluents in the visible light region is eminent. Although zinc oxide being a wide band gap material, responds to ultraviolet energy source; however, it can be altered to extend its response in the visible region. A comprehensive review regarding degradation of organic dyes via ZnO has been provided by Lam and et.al. [56]. The authors have summarized the research on ZnO photocatalytic systems for organic dyes degradation. The article discusses key operational parameters in the photocatalytic degradation and provided analysis regarding optimum operational parameters for improved photodegradation efficiency. It also shines light on enhanced degradation efficiency of modified ZnO in the visible region. A noteworthy attempt in summarizing visible light responsive ZnO based photocatalysts has been made by Pirhashemi, Yangjeh and Pouran in a review article [54]. The authors described advancements regarding binary and ternary ZnO based nanocomposites and heterostructures. In addition, Ahmed and et.al. [57], not only elaborated photocatalytic parameters and their effect but also discussed properties needed in an efficient photocatalyst.

Hence the two test dyes used for this research are:

- Methylene Blue
  ZnO nanostructures have been extensively used for degradation of MB dye and its related kinetic studies by monitoring adsorption processes [58, 59].
- Rhodamine B has dye has also been degraded and studied in detail by scientists and researchers [60].

There are numerous parameters involved in photocatalysis which significantly influence the outcome in dye degradation, and so, it is extremely difficult to find literature that matches all the parameters in one ‘s study, e.g. difference may occur in light source, its intensity, catalyst dose, pH, temperature, dye concentration etc. Hence, some of the results reported regarding MB and RhB degradation via ZnO has been summarized below in table 2.1and 2.2 respectively.

Table 2.1 Comparison of visible light photocatalytic degradation of MB dye in presence of ZnO nanostructures.

Sr. No.	Catalyst	Light Source	Concentration	Rate Constant (min^{-1})	Percentage Degradation	Time	Ref.
1.	ZnO NPs	500W Crown Bulb	$0.8gL^{-1}$ in 100mL of 10μM MB	0.0039	78%	480min	[61]
2.	ZnO Nanorods	Solar Simulator (AM 1.5G, 1 KWm^{-2})	3 cm x 1 cm Substrate in 10μM	Approx. 0.04	-	90min	[62]
3.	ZnO Nanorods	400W Sodium Lamp	250mg in 500ml of 5mg/L	-	99.3%	80min	[63]
4.	2% Nd doped ZnO Nanorods	500W Tungsten Halogen Lamp	200mL of 10ppm MB	0.288	100%	10min	[64]
	ZnO Nanorods			0.035	30%		
5.	ZnO/Au Hybrid	800 W Xe Lamp	0.1mg/mL in 20mL of 0.2mg/L MB	-	100%	80min	[65]
6.	ZnO Mesocrystals	500W Xe Lamp	40mg in 40mL of 10mg/L MB	-	85%	180min	[66]
7.	ZnO NPs	500W Halogen Lamp	3 cm x 1 cm Glass slide in 10μM MB	-	40%	180min	[67]
	ZnO Nanorods				60%		

Table 2.2 Comparison of visible light photocatalytic degradation of RhB dye in presence of ZnO nanostructures.

Sr. No.	Catalyst	Light Source	Concentration	Rate Constant (min^{-1})	Percentage Degradation	Time	Ref.
1.	ZnO Nanorod	Xe Lamp	10mg in 50mL of 10mg/L RhB	Approx. 0.006	92%	360min	[40]
2.	ZnO NPs	0.1W Hamamatsu LC8	1mg in 2mL of 5 x 10^{-6} M RhB	0.022	84%	120min	[68]
3.	ZnO Bumpy Spheres	300W Xe Lamp	0.1g in 100mL of 0.5 x 10^{-5} M RhB	-	92%	30min	[69]
4.	ZnO	Compact Fluorescent Lamp (CFL70 WBCB22)	50mg in 50mL of 1 x 10^{-5} M RhB	0.0073	52%	120min	[70]
	ZACP			0.0310	95%		

Chapter 3: Methodology

3.1 ZnO Nanoparticles

3.1.1 Materials

Zinc acetate dihydrate ($(CH_3COOH)_2Zn.2H_2O$; Daejung), zinc nitrate hexahydrate ($Zn(NO_3)_2.6H_2O$; BDH), zinc sulphate heptahydrate ($ZnSO_4.7H_2O$; Riedel-de Haën), sodium hydroxide (NaOH; Daejung), methylene blue ($C_{16}H_{18}CIN_3S.xH_2O$; Panreac), rhodamine B ($C_{28}H_{31}CIN_2O_3$; Alfa Aesar), ethanol (C_2H_5OH; 99.8 %, BDH) and hydrochloric acid (HCl; 37%, Riedel-de Haën) were utilized as received for experimentation. Moreover, distilled water was used for preparation of all aqueous suspensions.

3.1.2 Pilot-Scale Synthesis of Nanoparticles

Zinc oxide nanoparticles were prepared via coprecipitation technique stated by Pourrahimi in an article [71]. The reaction conditions were kept similar whereas, instead of using a glass reactor, simple lab apparatus was utilized for carrying out the reaction. The schematics of reaction setup is shown in figure 3.1.1.

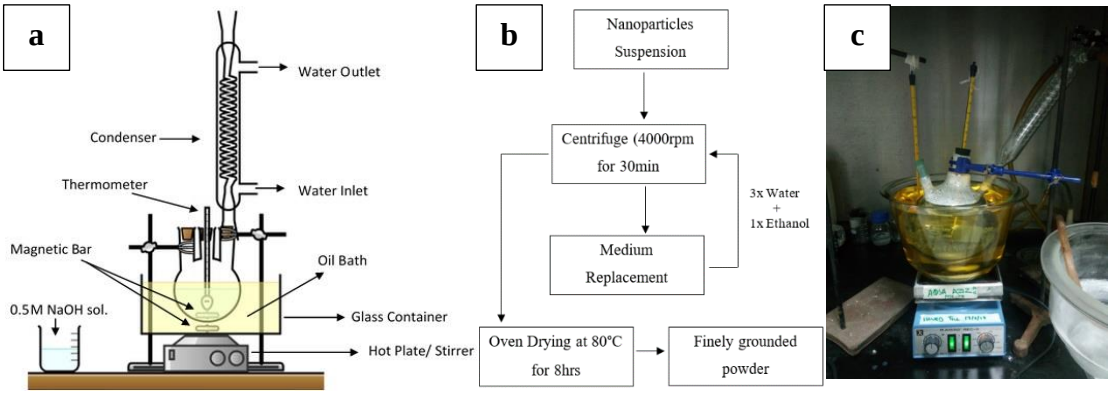

Fig. 3.1.1 (a) Experimental diagram for synthesis, **(b)** schematics of washing cycles of synthesized nanoparticles **(c)** synthesis setup for an experiment under process in lab.

In a typical experiment, 0.2 M zinc salt was added in 500 mL of distilled water in a three-neck round bottom flask, equipped with a reflux apparatus which was then placed in an oil bath. Microwavable glass bowl was used for oil bath with thermometer and a magnet bar placed in oil to ensure continuous stirring for temperature uniformity. Glass bowl was selected for oil bath because of its low thermal conductivity in comparison to metal containers henceforth allowing extremely good control over temperature. The zinc solution was then allowed to heat under vigorous stirring so that zinc salt dissolved

completely in water. When the temperature of the solution inside flask reached and stabilized at 60°C ± 0.5°C, separately heated aqueous solution of 0.5 M NaOH in 500 mL distilled water at 60°C was poured, at once, to the solution containing zinc salt precursor. On average, the addition of NaOH solution took only few seconds (approx. 5sec). The mole ratio of Zn^{2+}:OH^- ions as 1:2.5 was kept constant in all experiment. The pH of the solution was recorded as 13, at this point, using pH strips. The reaction was then allowed to proceed for an hour under vigorous stirring at 60°C. After synthesis, particles were cleaned via centrifugation at 4000rpm for 30min per cycle. 500ml plastic falcon tubes were filled with the prepared particles suspension for centrifugation while replacing the reaction medium with the same volume of distilled water after each centrifugation. Finally, the particles were centrifuged using ethanol as washing medium and the pH of particles lowered to neutral. After final centrifugation, the particles were dried at 80°C in lab oven for 8hours, and finally ground to a fine powder with a pestle and mortar. All samples yielded approximately 8g of white powdered which were labelled according to salt precursor and synthesis temperature.

3.1.3 Heat Treatment of Nanoparticles

The ZA-70 sample prepared using acetate salt precursor at 70°C was further subjected to heat treatment at three different temperatures 300°C, 550°C and 800°C in a muffle furnace. The Powder samples were transferred to crucible, covered, and then placed under ambient air at heating rate of 10°C min^{-1} for three hours of holding time. Heat treated samples were labelled after salt precursor, synthesis temp followed by heat treated temperature in parentheses. It's imperative to point out that sample heat treated at 550°C and 800°C changed their color from white to pale yellow upon heat treatment. Furthermore, the 800°C heat treated sample reverted to its primary white color when it cooled down to room temperature.

All the prepared samples are summarized in table 3.1 according to their synthesis conditions.

Considering the reaction conditions, the ions that take part in the whole process are yielded by dissociation of salt precursor and hydrolysis of base ions in zinc salt solution and NaOH solution respectively [26].

Zinc Salt Solution	NaOH Solution
$Zn(CH_3COO)_2{\cdot}2H_2O \longrightarrow Zn^{2+} + 2CH_3COO^- + 2H_2O$	
$ZnSO_4{\cdot}7H_2O \longrightarrow Zn^{+2} + 2SO_4^{2-} + 7H_2O$	$2NaOH \longrightarrow 2Na^+ + 2OH^-$
$Zn(NO_3)_2{\cdot}6H_2O \longrightarrow Zn^{2+} + 2NO_3^- + 6H_2O$	

Further reaction mechanism, due to presence of these ions, upon mixing of two solutions, can be presumed for zinc acetate dihydrate salt, by following chemical equations [19, 20, 47, 71].

$$Zn(CH_3COO)_2{\cdot}2H_2O + 2NaOH \longrightarrow Zn(OH)_2 + 2NaX + 2H_2O \quad (1)$$

$$Zn(OH)_2 + 2H_2O \longrightarrow Zn^{+2} + 2OH^- + 2H_2O \longrightarrow Zn(OH)_4^{2-} + 2H^+ \quad (2)$$

$$Zn(OH)_4^{2-} \longrightarrow ZnO + H_2O + 2OH^- \quad (3)$$

Similarly, equations can be written for other two salt precursors as well.

Table 3.1 Prepared ZnO samples, labelled according to synthesis conditions.

Sr. No.	Metal Salt Precursor	Synthesis Temperature	Sample Label
1.	$Zn(CH_3COO)_2{\cdot}2H_2O$	55	ZA-55
2.	$Zn(CH_3COO)_2{\cdot}2H_2O$	60	ZA-60
3.	$Zn(CH_3COO)_2{\cdot}2H_2O$	65	ZA-65
4.	$Zn(CH_3COO)_2{\cdot}2H_2O$	70	ZA-70
5.	$Zn(CH_3COO)_2{\cdot}2H_2O$	70	ZA-70 (300)
6.	$Zn(CH_3COO)_2{\cdot}2H_2O$	70	ZA-70 (550)
7.	$Zn(CH_3COO)_2{\cdot}2H_2O$	70	ZA-70 (800)
8.	$ZnSO_4.7H_2O$	55	ZS-55
9.	$ZnSO_4.7H_2O$	60	ZS-60
10.	$ZnSO_4.7H_2O$	65	ZS-65
11.	$ZnSO_4.7H_2O$	70	ZS-70
12.	$Zn(NO_3)_2{\cdot}6H_2O$	55	ZN-55
13.	$Zn(NO_3)_2{\cdot}6H_2O$	60	ZN-60
14.	$Zn(NO_3)_2{\cdot}6H_2O$	65	ZN-65
15.	$Zn(NO_3)_2{\cdot}6H_2O$	70	ZN-70

3.1.4 Characterization of Nanoparticles

3.1.4.1 XRD

Crystallinity and phase identification of prepared powdered nanoparticles was carried out using STOE Theta/theta X-ray Diffractometer System, equipped with Cu-Ka source of wavelength 1.54060 °A at a step size of 0.04 2θ.

3.1.4.2 TEM

Transmission electron microscopy TEM and scanning electron microscopy was utilized for morphology, defects and size analysis of samples.

3.1.4.3 SEM

For SEM (JSM-6490A, JEOL), extremely low concentration of nanoparticles was made in ethanol and bath sonicated for 30min, drop casted on glass slide, dried under lamp followed by very thin conductive Au sputtering. Samples were examined under 20kV accelerating voltage.

3.1.4.4 ATR-FTIR

Attenuated Total Reflection-Fourier Transform Infrared Spectroscopy (ATR-FTIR) measurements were carried out to investigate chemical nature of precipitates obtained after reaction as well as to study if there are any surface functional groups attached on ZnO nanoparticles. Measurements were taken by scanning powder samples using an AMTIR crystal element over the spectral range of 550cm^{-1} to 4000cm^{-1}.

3.1.4.5 UV-Vis Spectroscopy

Optical band gap as well as photocatalytic activities were calculated using absorption spectrum recorded via Jenway 7315 Spectrophotometer. For UV-Vis absorbance spectrum, typically 1.5mg ZnO sample was dispersed in 10ml ethanol via 30min bath sonication, from which 5ml was transferred into cuvette for analysis.

3.1.4.6 Photoluminescence

At room temperature photoluminescence (PL) emission measurements of powdered samples, in the spectral range 300 – 900 $nmcm^{-1}$, were made using HeCd laser line of excitation wavelength 325nm.

3.2 Photocatalytic Dye Degradation Evaluation

Room temperature photocatalytic activities of the samples were carried out under visible-light chamber designed in lab. The Fig. 3.2.1 shows the designed photocatalytic

chamber equipped with visible light source – 400W HPI-T Plus quartz metal halide lamp with clear outer bulb, a hot plate to keep suspension magnetically stirring and exhaust fans to lower the temperature inside the chamber. In a typical dye degradation experiment, know concentration of stock solution, for dye under investigation, was made. Desired volume of stock was taken and loaded with desired amount of ZnO catalyst followed by 10min bath sonication and placement on low magnetic stirring for sufficient time to ensure adsorption/desorption equilibrium of dye on the surface of ZnO nanoparticles. The suspension was then poured in glass petri dish and covered with glass to filter out any UV and infrared radiation by the light source and was then placed under irradiation source with stirring to maintain equilibrium. The distance between the light source and petri dish was 8inches, kept constant for all experiments. 5ml suspension was withdrawn via syringe every 10min, after irradiation followed by centrifugation to remove photocatalyst and finally its optical absorption spectra were taken using photo-spectrometer. The percentage degradation was calculated using:

$$Percentage\ Degradation = \frac{C_0 - C}{C_0} \times 100$$

Where, C_0 is the initial concentration and C is the concentration at a given time interval.

Fig. 3.2.1 Photocatalytic chamber equipped with 400W HPI-T lamp as a visible light source and exhaust fans to keep in check the temperature inside the chamber.

3.2.1 Methylene Blue

The photocatalytic degradation of methylene blue (MB) was carried out by dispersion of 60mg of ZnO photocatalyst in 60ml of 31.27mM MB stock solution. The photocatalytic activity of synthesized ZnO catalyst was evaluated and compared. ZnO catalyst showing the highest activity was further used to study effect of catalyst concentration and pH on the degradation of MB.

3.2.2 Rhodamine B

In addition, the sample showing the highest photocatalytic activity for methylene blue was also used to evaluate degradation behavior of rhodamine B dye. The photocatalytic degradation of rhodamine B was carried out by dispersion of 40mg of ZnO photocatalyst in 40ml of 50μM stock solution.

Chapter 4: Results and Discussion

4.1 Phase and Crystallinity

The phase and crystallinity of prepared ZnO samples were investigated via X-Ray diffraction. In Fig. 4.1.1 peaks appearing in the all ZnO samples corresponds to the miller indices of hexagonal wurtzite phase, which are in accordance with the available JCPDS reference code: 00-036-1451. Absence of any additional peaks is indicative of highly crystalline phase pure ZnO nanoparticles without any impurities.

A shift in (101) peak towards lower angles can be observed fig. 4.1.2 This is because increase in synthesis as well as heat treatment temperature shifts the diffraction peaks slightly towards the lower angles suggesting change in lattice parameters. In case of undoped ZnO, compression or expansion of lattice can occur due to either incorporation or removal of intrinsic zinc or oxygen related defects in the form of vacancies, interstitials, anti-sites etc. [72]. Characterization via photoluminescence spectroscopy has been used and discussed further in this chapter to investigate type and nature of these defects. Furthermore, the (101) peak intensity also increases depicting improvement in the overall crystallinity of the prepared samples. The lattice geometry equations for hexagonal structure are given by [73, 74]:

$$\frac{1}{d^2} = \frac{4}{3}\left(\frac{h^2 + hk + k^2}{a^2}\right) + \frac{l^2}{c^2}$$

$$a = \frac{\lambda}{\sqrt{3}\sin\theta}\left(\sqrt{h^2 + hk + h^2}\right) \quad \text{and} \quad c = \left(\frac{\lambda}{2\sin\theta}\right) l$$

$$Volume = 0.866 a^2 c$$

The crystallite size can be estimated using Scherrer equation for spherical particles, along with lattice strain as mentioned below:

$$\text{Crystallite Size} = \frac{0.89\lambda}{B\cos\theta} \quad \text{and} \quad \text{Lattice Strain} = \frac{B}{4tan\theta}$$

Where B is the structural broadening in radians, which is the difference in integral profile width between a standard and the unknown sample and given as:

$$B\ (size) = B_{obs.} - B_{std.} \quad \text{and} \quad B\ (strain) = \sqrt{{B_{obs.}}^2 - {B_{std.}}^2}$$

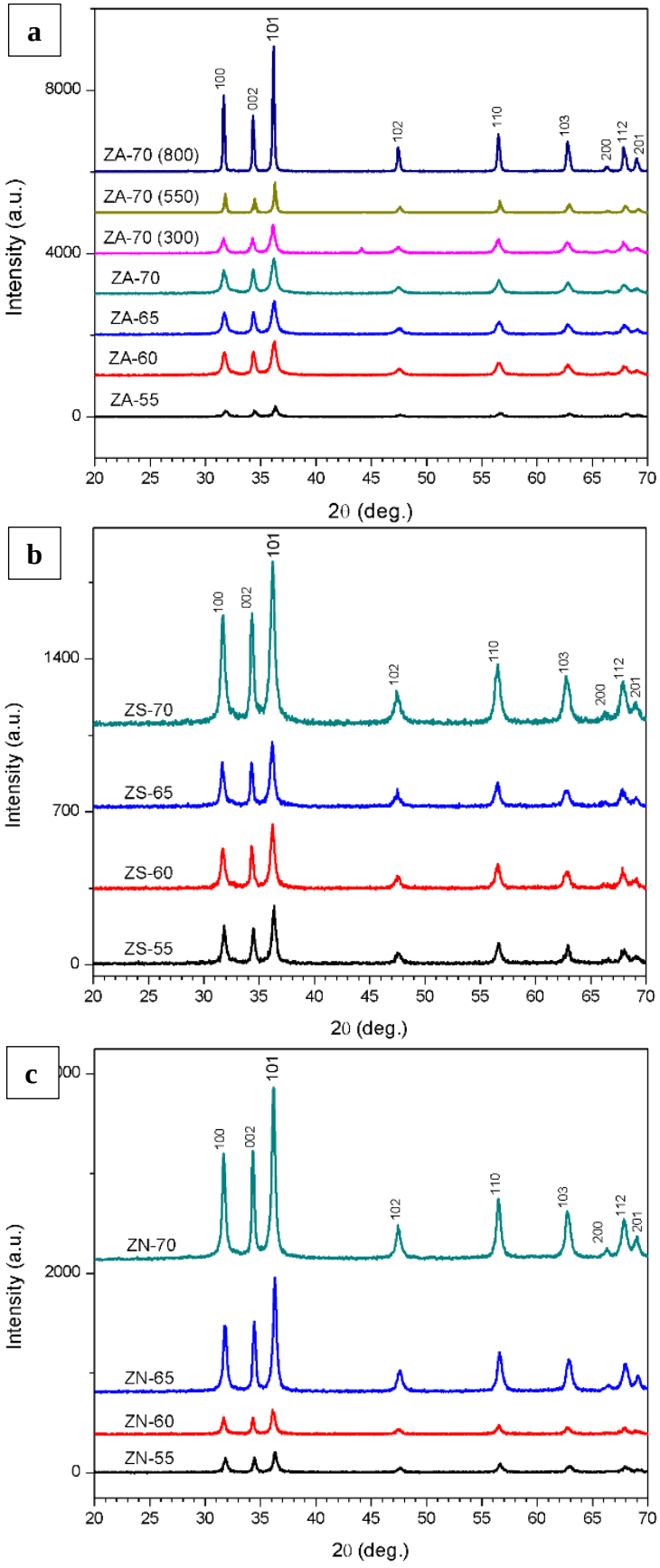

Fig. 4.1.1 X-ray diffractograms of synthesized ZnO nanoparticles.

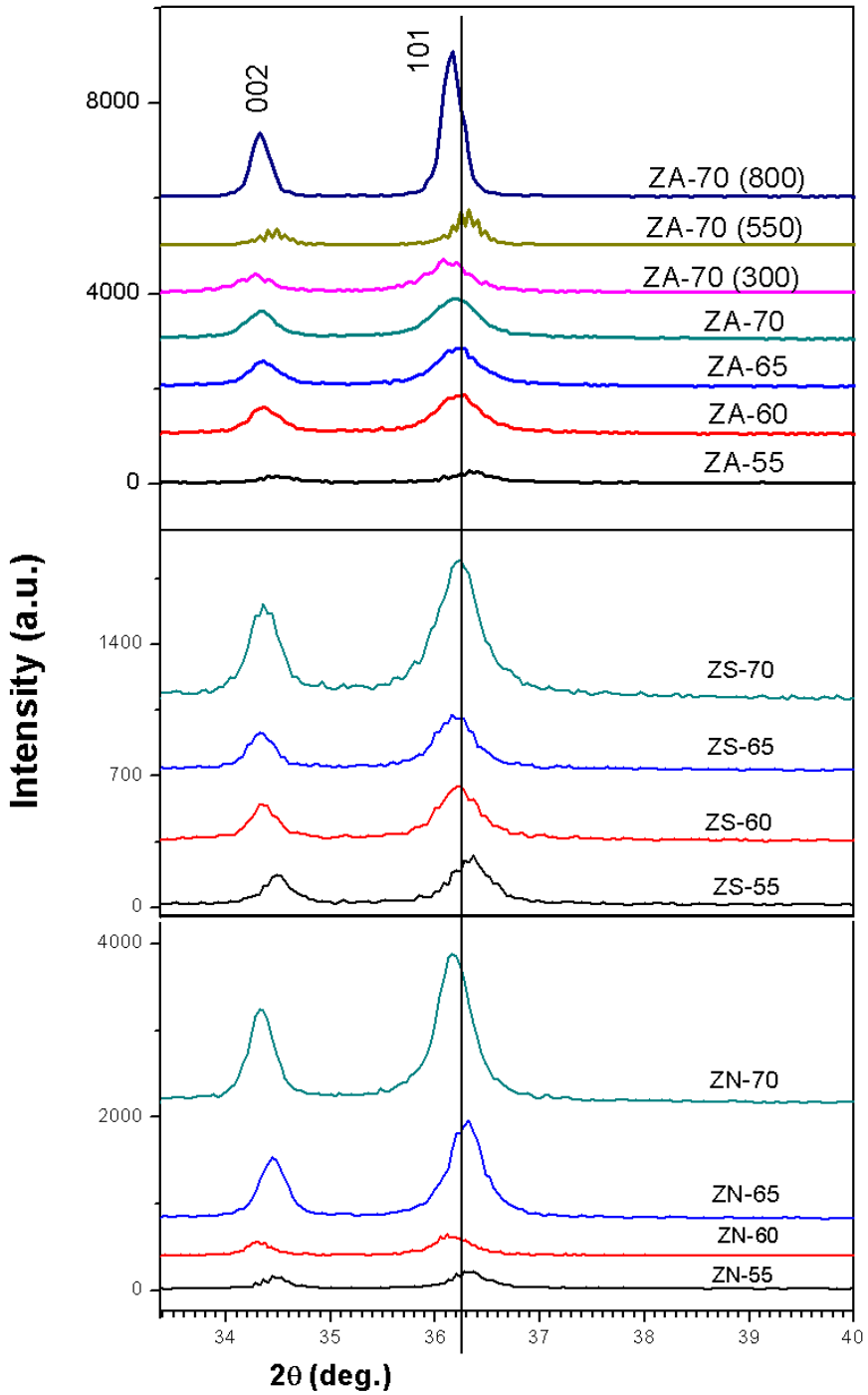

Fig. 4.1.2 Shift in (101) peak as result of difference in synthesis conditions.

Lattice constants ‘a’ and ‘c’ were calculated from peaks 100 and 002 respectively. The peaks in the diffractogram were indexed and calculations regarding crystal structure have been summarized in table 4.1. The two noteworthy observations regarding calculated crystallite sizes from the table are:

1. With respect to synthesis temperature we can see that at 60°C the prepared nanoparticles have same crystallite size irrespective of the salt precursor used.

Whereas, for the rest of synthesis temperatures i.e. 55°C, 65°C and 70°C, this trend holds true only in case of sulphate and nitrate salt precursors showing deviation for acetate derived particles.

2. With respect to salt precursor used for synthesis it is evident that variation in crystallite size of acetate samples as a function of synthesis temperature is quite wide in comparison to sulphate and nitrate. Moreover, the crystallite size further increased upon heat treatment of ZA-70 sample. This is because heat treatment allows atomic mobility and therefore atoms can move to energetically favored sites such as voids, interstitials and grain boundaries causing relaxation in crystal lattice thus improving crystallinity (as shown by increase in peak intensity) and decreasing the lattice strain in samples. It shows that the lattice strain decreases with the increase in heat treatment temperature.

In most wurtzite ZnO structures the c/a ration is smaller than the ideal value of 1.633, reason being electrostatic attraction between the pairs of cation and anion atoms present along the [0001] direction makes it more stable than the other zinc blend structure exhibited by zinc oxide [9]. Therefore, the difference between ideal and calculated c/a ratio of prepared samples insinuates the possibility ionic species present on the surface of prepared ZnO nanoparticles.

Table 4.1 Prepared samples lattice parameters calculated from Xrd diffractograms using X'Pert HighScore software and crystal geometry equations.

Samples	Peak Position [°2Th.]	FWHM [°2Th.]	d-Spacing [Å]	Crystallite Size [Å]	Lattice Strain [%]	a [Å]	c [Å]	c/a Ratio	Volume [Å]^3
JCPDS Card	36.253	-	2.476	-	-	3.250	5.207	1.602	47.620
ZA-55	36.381	0.197	2.469	707	0.239	3.239	5.209	1.608	47.330
ZA-60	36.252	0.354	2.478	302	0.460	3.257	5.221	1.603	47.957
ZA-65	36.273	0.315	2.477	352	0.406	3.254	5.217	1.603	47.833
ZA-70	36.199	0.472	2.481	211	0.621	3.260	5.217	1.600	48.020
ZA-70 (300)	36.059	0.276	2.491	424	0.353	3.257	5.229	1.606	48.020
ZA-70 (550)	36.318	0.197	2.474	707	0.239	3.247	5.199	1.601	47.460
ZA-70 (800)	36.134	0.236	2.486	530	0.297	3.259	5.224	1.603	48.044
ZS-55	36.355	0.315	2.471	352	0.405	3.242	5.198	1.603	47.301
ZS-60	36.202	0.354	2.481	302	0.460	3.258	5.218	1.602	47.968
ZS-65	36.270	0.315	2.477	352	0.406	3.261	5.226	1.602	48.142
ZS-70	36.245	0.315	2.478	352	0.406	3.254	5.226	1.606	47.931
ZN-55	36.357	0.315	2.471	352	0.405	3.240	5.203	1.606	47.288
ZN-60	36.125	0.354	2.486	302	0.461	3.261	5.223	1.602	48.086
ZN-65	36.354	0.276	2.471	424	0.350	3.247	5.205	1.603	47.517
ZN-70	36.132	0.315	2.486	352	0.408	3.258	5.221	1.602	48.000

4.2 Morphology and Size

Fig. 4.2.1 shows transmission micrograph of two prepared samples and clearly indicates that particles are of spheroidal morphology and highly agglomerated. It can be seen that Sample ZA-60 exhibits nanoparticles of smaller size in comparison to ZN-65. This is possibly due to two reasons; one that increase in synthesis temperature increases the size of nanoparticle, and second the change in salt precursor affects the size of particle because of difference in chemistry of anions involved. The second point of view has been deliberated by Pourrahimi and et.al [71] stating that the acetate ion, present in zinc acetate salt precursor, is positively charged methyl functional unit which can act as an amphiphilic capping layer around nanoparticles to prevent possible growth by fusion of particles. Whereas in comparison sulphate and nitrate salt precursors consist of ions with significantly smaller coordination capacity and there are no carbon functional units present.

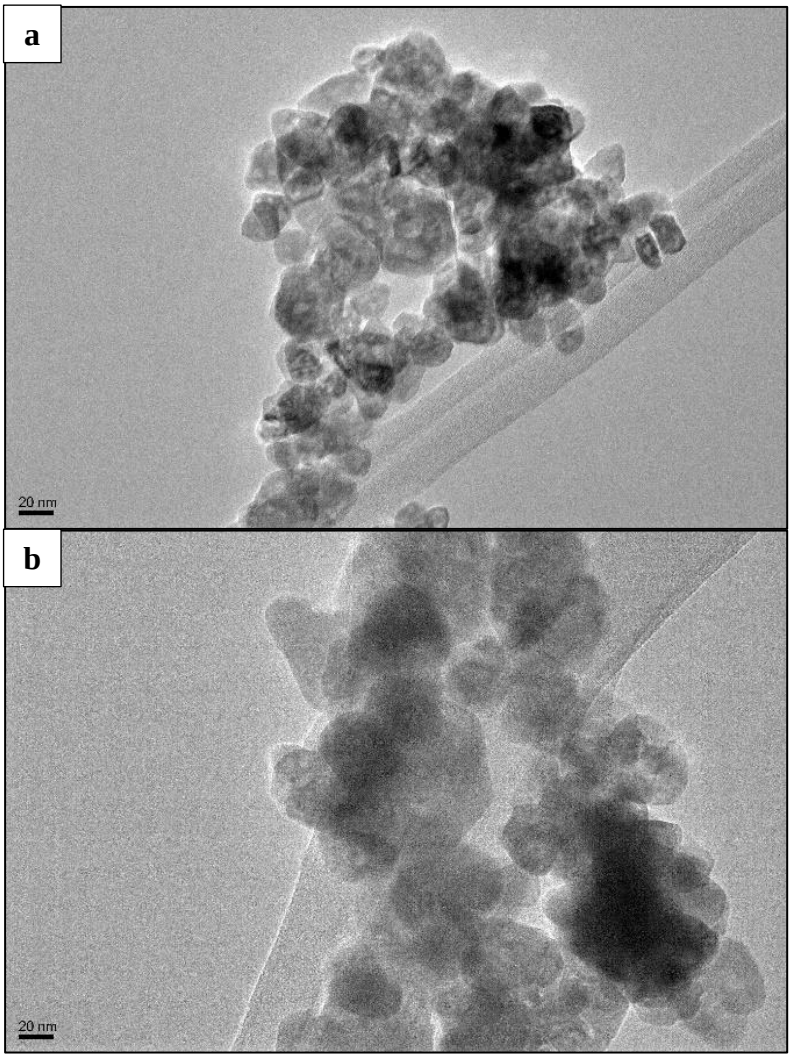

Fig. 4.2.1 TEM micrographs of ZnO nanoparticles **(a)** sample ZA-60, derived from zinc acetate at 60°C and **(b)** sample ZN-65, derived from zinc nitrate at 65°C.

This observation is somewhat comparable to the crystallite sizes of nanoparticles calculated via XRD analysis. It has been noted that size variation of acetate derived particles is abruptly larger, as a result of temperature variation, in comparison to sulphate or nitrate. Hence, this suggests that the capping action of carbon functional group is probably temperature dependent and it increases with the increase in synthesis temperature. As XRD analysis reveals that sample ZA-70 shows the lowest crystallite size of 21.1 nm amongst all prepared samples and sample ZA-55 has the highest crystallite size of 70.7 nm. Therefore, role of precursor cannot be neglected. However, more insight into thermodynamics and chemistry related kinetics, of a particular salt precursor, is needed for better understanding of salt precursors' effect on nanoparticles.

TEM was further utilized to investigate the planar defects present in both the samples. Fig. 4.2.2 shows that both samples contain high density of dislocations. The reflux setup in oil bath kind of provides a close environment with minimum temperature variations keeping the reaction system in constant source of thermal agitation. This is all possible because the oil surrounding the flask is kept at the same temperature. Whereas, in comparison setups using beakers without oil bath and reflux bring in huge thermal variations as the environment of beaker is at different temperature, i.e. lower than the solution allowing heat exchange with the environment so that it can reach equilibrium. Furthermore, adding concentrated NaOH solution, at once, to the zinc precursor solution provides a pH shock which not only triggers instantaneous nucleation but simultaneous growth as well. Hence, dislocations stem in order to relieve the strain induced in the crystal lattice because of synthesis setup and the parametric reaction kinetics.

The XRD analysis show high lattice strain values also support that the growth is indeed dislocation driven [75]. Although literature reports several articles for planar defects, such as edge, screw and threading dislocation, stacking faults and twinning, in nanoparticles [76, 77] but screw dislocations in undoped ZnO nanoparticles via solution-based synthesis have not been reported as per our knowledge. Rather the limited amount of literature for screw dislocations is based on one- and two-dimensional zinc oxide nanostructures [78-80]. Couple of reports regarding planar defects in ZnO nanoparticles includes nanoparticles' synthesis via laser ablation [81] and polymorphic transformation [82].

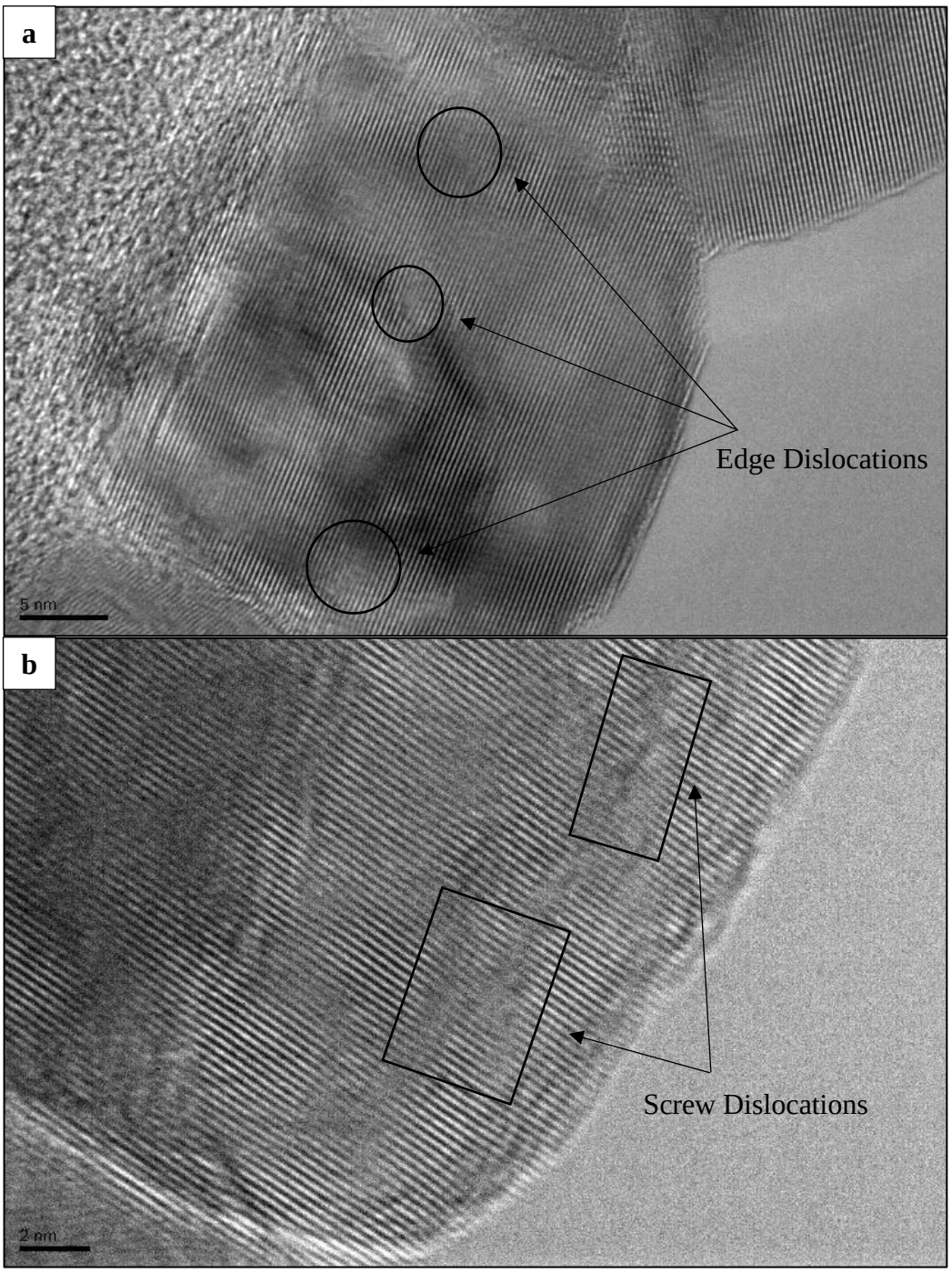

Fig. 4.2.2 Marked dislocation defects in nanoparticles **(a)** ZA-60 and **(b)** ZN-65.

Morphology of all prepared sample was investigated by SEM images shown in Fig. 4.2.3. All prepared nanoparticles exhibit spherical morphology and are well within nanometer range. It is interesting to note that the large sized agglomerated nanoparticles, as shown in TEM image (Fig.4.2.1 for sample ZA-60 and ZN-65), disintegrated into smaller monodispersed nanoparticles when sonicated in ethanol for SEM analysis.

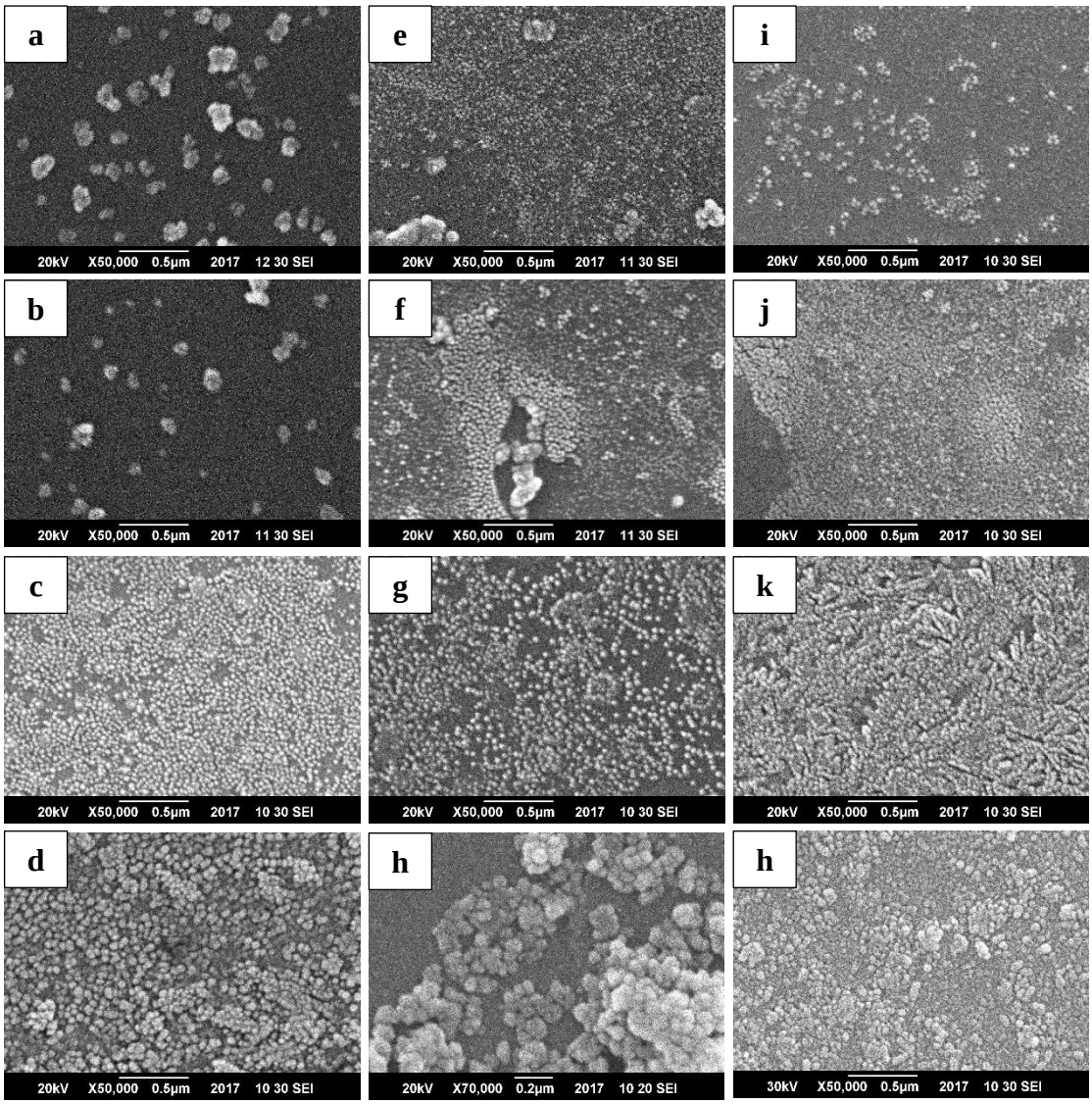

Fig. 4.2.3 SEM images of prepared nanoparticles using salt precursors at various temperatures using acetate at **(a)** 55°C, **(b)** 60°C, **(c)** 65°C, **(d)** 70°C; using sulphate at **(e)** 55°C, **(f)** 60°C, **(g)** 65°C, **(h)** 70°C; using nitrate at **(i)** 55°C, **(j)** 60°C, **(k)** 65°C, and **(l)** 70°C.

4.2.1 Growth Mechanism

The general synthesis mechanism can be explained according to the reactions mentioned in section 3.1.2. The nucleation is triggered via Zn^{2+} ions as they undergo hydroxylation due to presence of OH^- ions, forming a white precipitate, $Zn(OH)_2$.

$$Zn^{2+} + 2OH^- \longleftrightarrow Zn(OH)_2 \quad (1)$$

The above reaction is immediately followed by the formation of zincate ion, a water-soluble growth unit in the form of $Zn(OH)_4^{2-}$ as $Zn(OH)_2$ dissolves due to excess of OH^- ions which raises pH of the solution [83-85].

$$Zn(OH)_2 + 2H_2O \longrightarrow Zn^{2+} + 2OH^- + 2H_2O \longrightarrow Zn(OH)_4^{2-} + 2H^+ \quad (2)$$

There are several zinc growth species that can lead to formation of ZnO, such as Zn^{2+}, $Zn(OH)^+$, $Zn(OH)_2$, $Zn(OH)_3^-$, $Zn(OH)_4^{2-}$ or polynuclear zinc complex as $Zn_2(OH)^{3+}$, $Zn_2(OH)_6^{2-}$, depending upon the synthesis process and physical factors such as temperature, concentration of ions and pH. However, it is well documented that at pH > 12, the dominant zincate ions are $Zn(OH)_3^-$ and $Zn(OH)_4^{2-}$, with $Zn(OH)_4^{2-}$ ions relatively more abundant, hence the reason it's stated above that $Zn(OH)_4^{2-}$ is the responsible growth unit in ZnO formation [17, 24, 68, 86, 87].

The addition of NaOH solution into salt precursor solution, at once, increases nucleation sites for particle growth by rapidly producing zinc hydroxide species followed by ZnO formation via decomplexation in a short time. Due to higher mole ratio of Zn^{2+}:OH^- ions (1:2.5 with pH=13 in experiments performed), the high OH^- ion concentration rapidly drives conversion of Zn(OH)2 to ZnO, allowing coarsening of ZnO by the equilibrium dissolution/re-crystallization processes in the solid–liquid system. In addition, $Zn(OH)_4^{2-}$ and OH^- ions concentration influences the ZnO crystallite's morphology as well as controls growth rate of different crystal faces [88]. Whereas, increase in temperature increases nuclei formation resulting in smaller particles and decreases the relative stability of zinc-hydroxide species in comparison to ZnO, leading to its increased precipitation [17]. Interestingly, NaOH not only provides hydroxyl ions necessary for carrying out growth of ZnO, it also provides Na^+ counterion that reportedly impedes growth by acting as capping agent via hindering Zn^{2+} ions approach towards nanocrystal's growing surface [89].

4.3 Optical Properties

4.3.1 Functional Groups or Salt Residue

In order to identify presence of any residual salt precursor or functional groups, the IR spectrum of prepared samples was acquired in the range 550 – 4000 cm^{-1}, shown in Fig. 4.3.1. Four major bands appeared in all the prepared samples and justification of their presence is well documented in literature. A broad and weak band in the range 3100 – 3600 cm^{-1} is an indication of O–H stretching vibration mode of the hydroxyl groups due to water adsorbed by ZnO powders but taken together with the blimp in the range 1615 – 1640 cm^{-1}, confirms presence of traces of water. The hygroscopic nature of ZnO also supports the aforementioned observation [31, 90-93]. Furthermore, the two types of OH interactions on the surface of ZnO nanoparticles available in literature are the reversible dissociative adsorption of hydrogen on both O and Zn sites (3000 – 3650 cm^{-1} band) and the chemisorbed water (1610 – 1630 cm^{-1} band) [94]. A band in the range 1210 – 1410 cm^{-1} is attributed to the in-plane OH bending vibrations [92]. Another peak that appeared in all samples around 880 cm^{-1} emanated from the stretching vibration of Zn–OH as a result of tetrahedral coordination of Zn [32, 94].

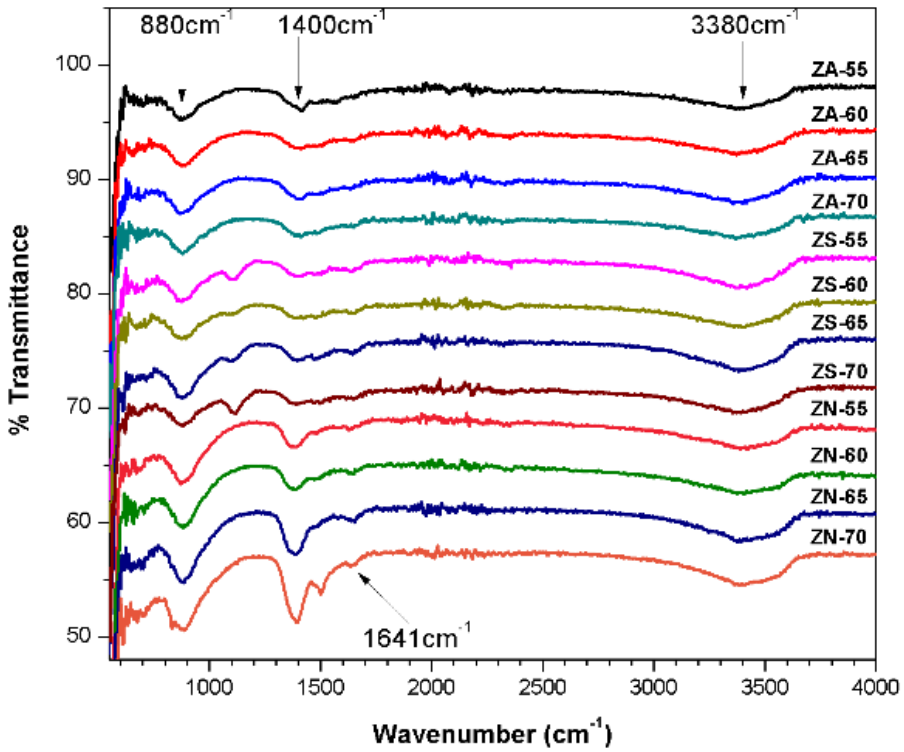

Fig. 4.3.1 ATIR Spectra of prepared ZnO samples showing four major peaks.

Apart from the above-mentioned bands, samples prepared from sulfate and nitrate precursors show additional peaks. The peak in the region 1080 – 1130 cm^{-1} appearing

only in ZS-d and ZS-c, prepared from zinc sulfate salt, suggests the remnants of sulfate ions even after washing of nanoparticles [25, 92]. Similarly, in sample ZN-c, made from zinc nitrate salt precursor, the peak in the region 1430 – 1500 cm^{-1} is due to presence of nitro compounds [92]. Both these sulphate and nitrate ions are present only in trace amount i.e. low enough that no impurity peak arises in x-ray diffractogram due to them.

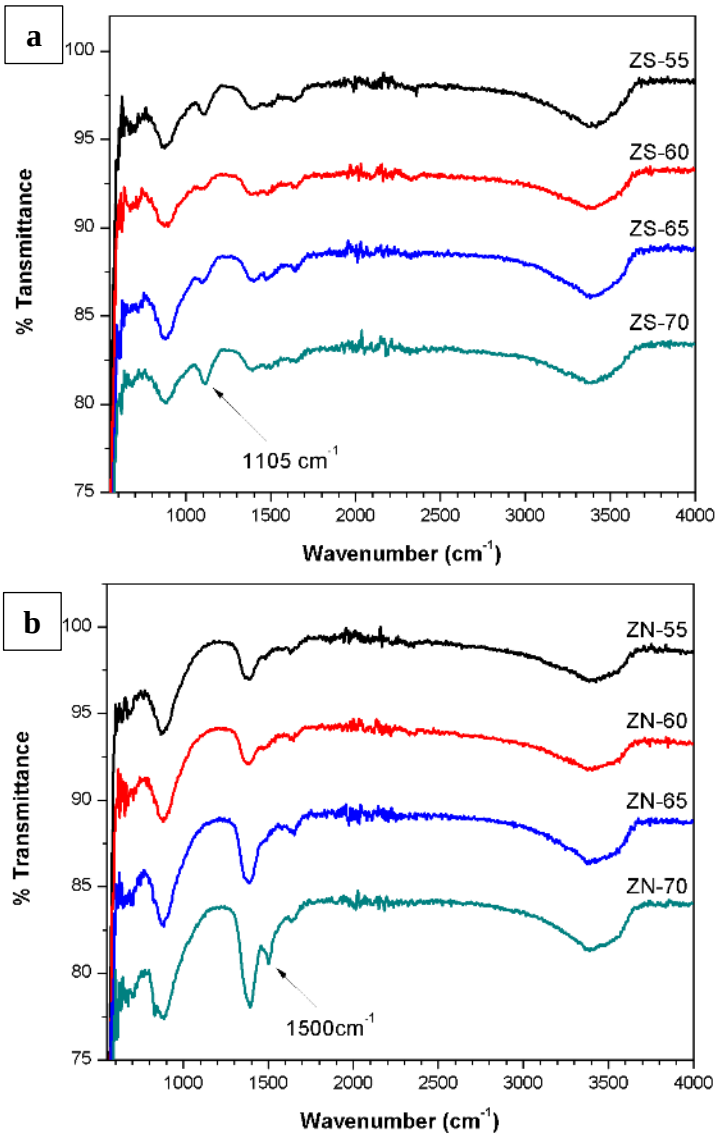

Fig. 4.3.2 ATIR Spectra of ZnO samples from **(a)** sulfate precursor and **(b)** nitrate salt precursor showing additional peaks at ~1105cm^{-1} and ~1500cm^{-1} respectively.

Table 4.2 Identified IR peak positions for prepared samples along with reference to the functional groups present.

Characteristic Bands (cm^{-1})	Sample Peak Positions (cm^{-1})										Functional Group	
	ZA-55	ZA-60	ZA-65	ZA-70	ZS-55	ZS-60	ZS-65	ZS-70	ZN-55	ZN-60	ZN-65	ZN-70
~880	876.7	874.6	868.4	876.7	874.6	893.1	878.7	876.7	868.4	880.8	884.9	884.9	Zn–OH Stretching
1080 – 1130	-				1105.1	-		1117.4					Sulphate ions
1260 – 1410	1415.8	1409.7	1397.3	1411.7	1405.5	1422.0	1397.3	1393.2	1380.9	1387.0	1385.0	1393.2	O–H Bending
1430 – 1500	-				-					-		1500.2	Nitro Compounds
3100 – 3600	3370.8	3370.8	3356.4	3368.8	3418.2	3362.6	3383.2	3354.4	3426.4	3405.8	3374.9	3387.3	Water of Crystallization

4.3.2 Bandgap

Optical properties were investigated using UV-Vis and are based upon absorption spectrum as a function of wavelength [95, 96], shown in Fig. 4.3.3. The absorption coefficient, near the absorption edge, is given by:

$$(\alpha h\upsilon)^{1/n} = h\upsilon - E_g$$

Where '$h\upsilon$' is photon energy, α is absorption coefficient and 'n' is a constant whose value depends upon transition characteristic in a semiconductor (n= 1/2, 2, 3/2 or 3). For ZnO n = 1/2, due to allowed direct transition. A graph, termed as Tauc plot, between $(\alpha h\upsilon)^2$ as ordinate and photon energy ($h\upsilon$) as abscissa is plotted and extrapolation of its linear region gives the bandgap energy.

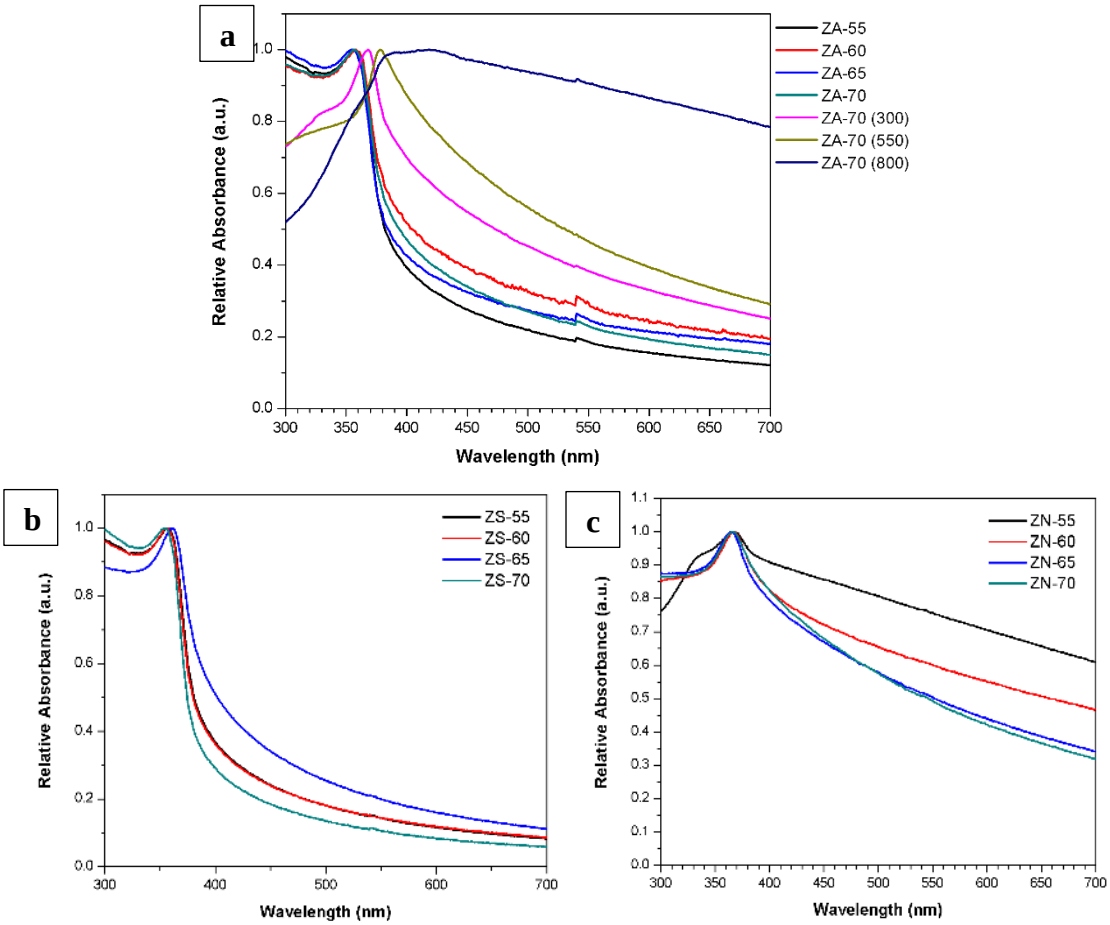

Fig. 4.3.3 UV-Vis absorption spectra of prepared ZnO samples from **(a)** acetate precursor **(b)** sulphate precursor and **(c)** nitrate precursor.

Fig. 4.3.4 shows bandgap energies of prepared nanoparticles obtained via Tauc plots and are summarized in table 4.3. It is evident that prepared nanoparticles are of lower bandgap energies than bulk ZnO (3.37eV).

Series of nanoparticles prepared from acetate have closely related bandgap energies, and the same holds true for sulphate and nitrate salt precursors. It can be seen in Fig. 4.3.3 that UV-Vis spectra of samples obtained via nitrate precursor show absorption spectra tailing into the visible region and similar result for ZnO obtained via nitrate and chloride precursor has been seen in a study by Srikanth [25] comparing chloride, nitrate, sulphate and acetate salt precursors. The closely related bandgap values are possibly because of the overlapping of the valence band-donor levels because of surface states. Also, calculated energy values show that choice of salt precursor affects the bandgap value of ZnO nanoparticle, here the order of bandgap values for prepared nanoparticles is: E_g of nitrate precursor derived nanoparticles < sulphate precursor derived nanoparticles < acetate precursor derived nanoparticles (ZN < ZS < ZA).

However, when sample ZA-70 was heated treated at different temperatures there is a red shift in absorption peak of UV-Vis spectra to longer wavelengths and the absorption edge increases to higher wavelength with increase in heat treatment temperature (300℃ to 800℃). As a result there is a remarkable reduction in bandgap

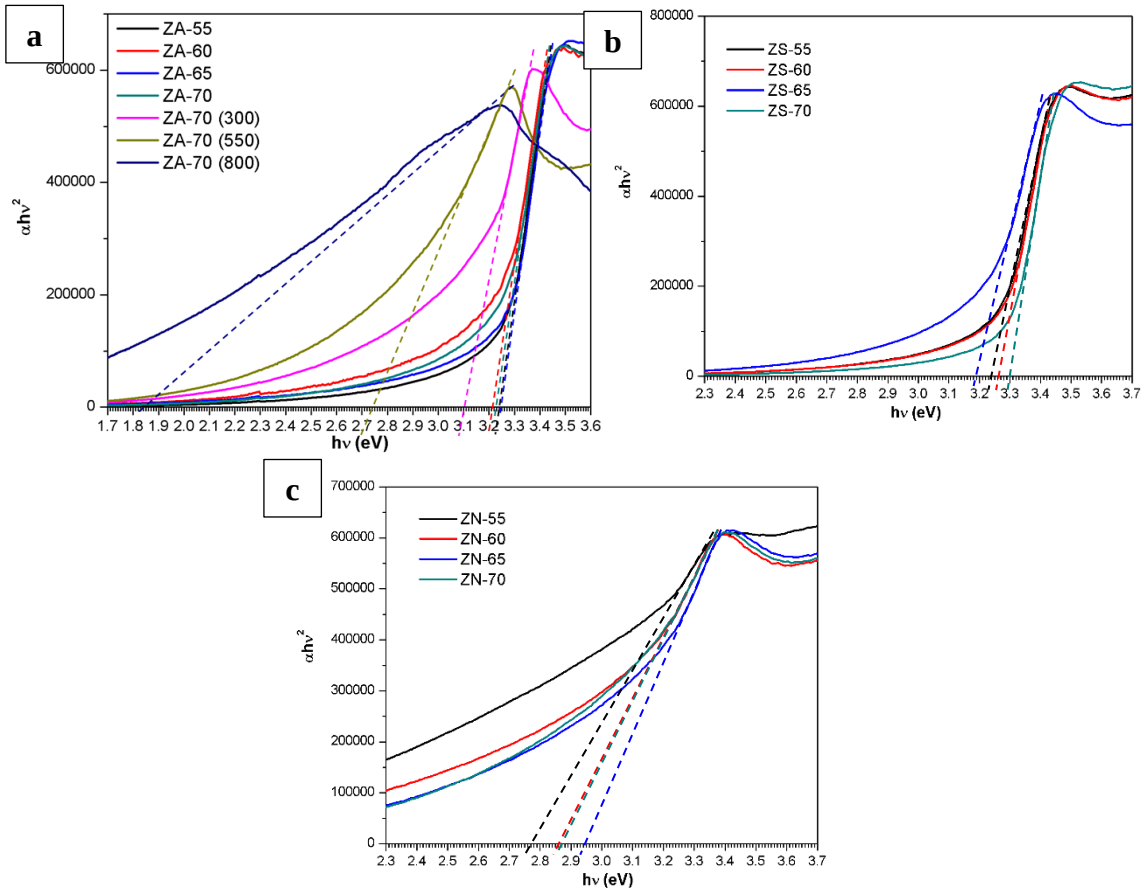

Fig. 4.3.4 Tauc plots of all prepared sample from **(a)** acetate **(b)** sulphate and **(c)** nitrate salt precursor.

energies, this is because heat treatment has a pronounced effect on defect's type and concentration, such as planar and surface defects present in the form of dislocations, vacancies and interstitials, etc. [30, 34]. Furthermore, its noteworthy that upon heat treatment at 550°C and 800°C the white ZnO powder changed color to pale yellow, although the 800°C treated sample changed back again to white after it cooled down to room temperature, whereas ZA-70 (550°C) remained pale yellow. This color change is shown in Fig. 4.3.5. Similar observations regarding color variation has been previously reported by Wang, et.al [97] and Peng, et.al [66] in their respective articles and both associated this with oxygen defect concentrations.

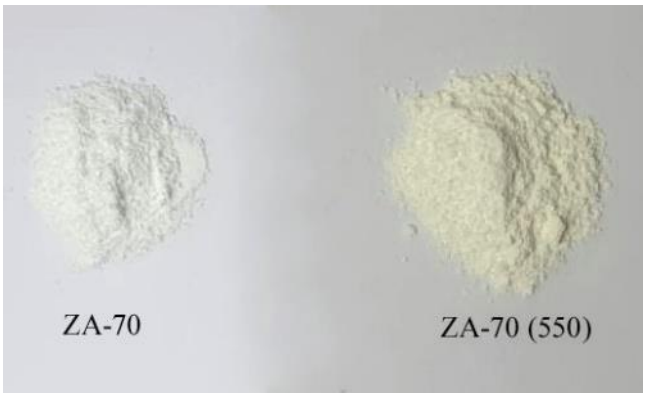

Fig. 4.3.5 Color change in a prepared ZnO sample upon heat treatment.

Table 4.3 Bandgap energies of prepared ZnO nanoparticles.

Sr. No.	Prepared ZnO Samples	Band Gap (eV)
1.	ZA-55	3.24
2.	ZA-60	3.22
3.	ZA-65	3.25
4.	ZA-70	3.23
5.	ZA-70 (300)	3.10
6.	ZA-70 (550)	2.74
7.	ZA-70 (800)	1.84
8.	ZS-55	3.24
9.	ZS-60	3.26
10.	ZS-65	3.19
11.	ZS-70	3.30
12.	ZN-55	2.77
13.	ZN-60	2.86
14.	ZN-65	2.87
15.	ZN-70	2.95

4.3.3 Defects

Characterization of defects present in ZnO can be explained in a comprehensive way via photoluminescence phenomenon. For this purpose, the PL spectra for all the prepared powder samples were recorded using He–Cd laser of wavelength 325nm. The graphs in Fig. 4.3.6, for all samples, can be divided into two main regions; (i) UV region peak centered approx. at 400 nm and (ii) Visible region broad peak centered approx. at 580nm, consisting of several smaller peaks. The sharp and intense peat a ppearing at approximately 645nm is ZnO Raman [98].

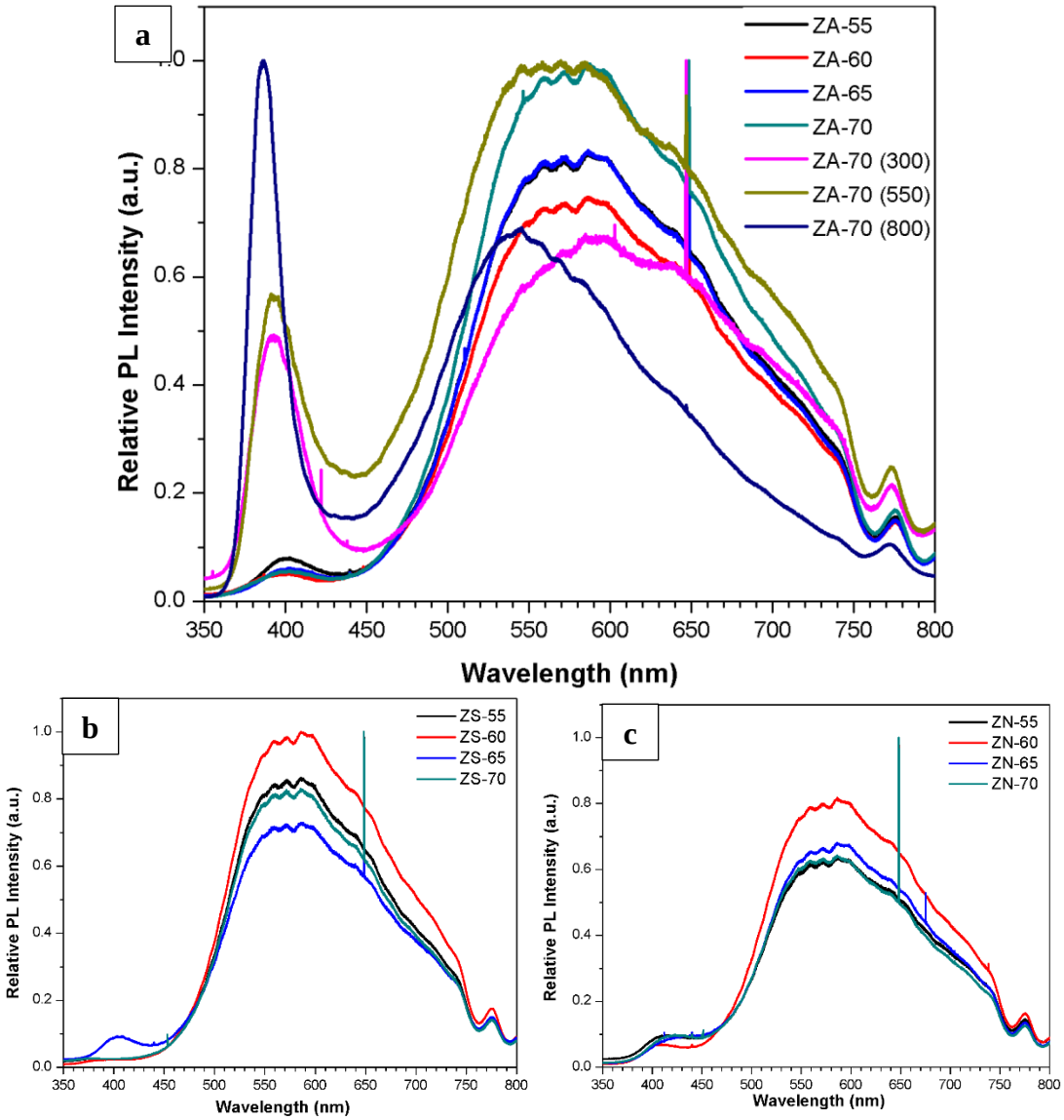

Fig. 4.3.6 Room temperature PL spectra under HeCd (λ = 325nm) excitation, of all prepared ZnO samples using **(a)** acetate; **(b)** sulphate; and **(c)** nitrate salt precursor.

ZnO usually exhibit UV region peak (λ<4 00nm) due to excitonic band to band transition near the bandgap (also NBE i.e. near-band-edge emission) and visible region peak for defect concertation of various types and is responsible for deep level green,

yellow or red emission [30, 68]. It can be seen in the Fig. 4.3.6 that as prepared samples do not show any peak in the ultraviolet region of the electromagnetic spectrum, and it only appears in heat treated samples. Absence or a very weak exciton emission in ZnO have been reported in literature [43, 45, 99, 100] and Zhang expressed in his study [88] that high density of surface defects compromises the crystal quality of nanostructured ZnO, which accounts for UV emission quenching and hence only defects related visible emission appears in Pl spectra. In addition, Wang reported that entrapment of photoinduced electrons into oxygen vacancy (V_o) level defect, facilitates charge separation preventing recombination which results in absence of intrinsic UV emission [40]. In this study however, we believe the ~400nm peaks of prepared samples result from excitonic emission whose range has been widen to violet region because of high pH synthesis environment of nanoparticles, as suggested by [20]. Similar violet ranged excitonic emission has been reported by Wu [47] for urchin/flower-like ZnO nanostructure and by Thi Do for Pd-doped ZnO nanoparticles [48].

Violet emission occurs as a result of transition from zinc interstitial Zn_i to the VB. The theoretical calculations show that Zn_i lies 0.22eV below CB [52]. The most commonly observed emission in ZnO is the green emission which has been linked to various defects such as oxygen vacancies (charged or neutral) [34, 43, 49, 50, 101-106], zinc vacancies (V_{Zn}) [44], oxygen anti-sites [107] etc. Here, the green emission has been assigned to transition between Zn_i to V_o and it can be seen that the emission is persevered up to a certain degree even upon heat treatment of the sample. Yellow emission at 578nm (2.14 eV) and orange emission at 600nm (2.06 eV) likely emerge from the presence of hydroxyl group (–OH) or non-converted Zn(OH) on the surface of nanoparticles [42, 44]. This has been further supported by Vempati [106] by stating that yellow-orange emission involves radiative transition from OH states to deep-lying states (or possibly the VB edge). Although yellow-orange emission has also been credited to oxygen interstitials [52] but its association in this research with hydroxyl group is more convincing since our ATIR results also support presence their presence. Finally moving on towards the longer wavelengths, the most noticeable red emission is the intense peak at 649nm (1.91 eV) along with the weaker emission at 775nm (1.599 eV). Red emission has been linked with singly ionized oxygen vacancies (V_o^+) [108], zinc vacancies [109], oxygen interstitials [110] and lattice disorder along c-axis [111] as well as with thread dislocations [112]. Nanoparticles prepared in this research have

high concentration of dislocation as shown by TEM analysis, so it is believed that the red emission here is associated with lattice disorder in addition to the excess of surface oxygen.

In Fig. 4.3.6 (a), The ZA-70 sample has the highest PL intensity and rest of the samples' Pl spectra are replica of it with the only difference in their relative intensities. This shows that the defects are controlled and reproducible. It is evident that sample prepared from acetate salt precursor has the highest density of defects followed by sulphates and nitrates (ZA>ZS>ZN), similar trend was reported by Pudukudy and Yaakob [27]. Furthermore, it also shows that increase in annealing temperature increases the UV emission of nanoparticles and also shows blue shift because of recovery of dislocated atom and reduction in point defects and is in accordance with the XRD results. Whereas, visible emissions do not show this trend. The visible emission intensity dropped considerably when sample ZA-70 was annealed at 300°C, but the sample remain unchanged when it was subjected to higher annealing temperature of 550°C. When annealing temperature was raise to 800°C, the visible emission intensities dropped more so than 300°C heat treatment. Most considerable drop is for yellow, orange and red emissions. This shows that the red emission is indeed due to lattice related defects which improved upon heat treatment as nanoparticles not only show growth in size but also show improvement in overall crystallinity of the material as well. These results are well in agreement with our XRD analysis as it showed better crystallinity, increased crystallite size and less lattice strain upon heat treat of nanoparticles. Hence, annealing not only affects the density of defects present but it also brings change to the types of defects in a sample. Furthermore, the defect responsible for the green emission remained present, although in less concentration than pristine sample, even after annealing at as high as 800°C temperature. And despite the fact there is no consensus regarding responsible entity for green emission, it has stated by Djurišić and Leung [113] that there is convincing evidence that emission is related to the defect present at the surface of ZnO.

4.4 Photocatalytic Activity of ZnO NPs

4.4.1 Methylene Blue Degradation

MB, one of the mainstream organic pollutant, found in waste-water discharge by textile industries, was selected to assess photocatalytic efficiency of ZnO NPs under visible

light irradiation. According to Beer–Lambert law, the relative concentration (C/C_0) of the MB solution was calculated by the relative absorbance (A/A_0) at characteristic absorption value of MB observed at 664nm. Under dark conditions with the presence of catalyst MB demonstrated very little dye degradation owing to adsorption of dye on the catalyst surface. Control experiments show that prepared samples degraded MB dye as signified by decrease in the characteristic absorbance at 664nm and decolorization, as shown in fig. 4.4.1. The kinetic investigations were carried out for understanding of photodegradation process. The graphs of $\ln(C/C_0)$ vs. irradiation time (t) for MB plotted a good liner fit, with R^2 (correlation coefficients) values higher than 0.9, indicating pseudo-first-order kinetics followed by NPs for photodegradation of MB. It's a simplified form of Langmuir–Hinshelwood (L–H) model if the concentration of reactant is very low i.e. KC << 1 (where K and C are adsorption equilibrium constant and concentration of the reactant, respectively) [64, 68]:

$$-\ln\frac{C}{C_0} = kt$$

Where k is the apparent pseudo-first-order rate constant (min^{-1}), t is reaction time, C_0 is the initial concentration and C is the concentration at time t, of the reactant.

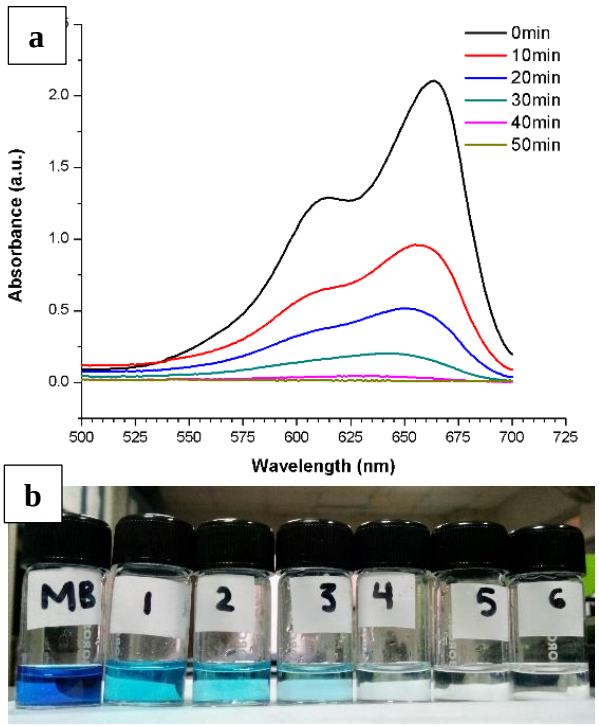

Fig. 4.4.1 MB degradation shown via **(a)** decrease in 664nm peak and **(b)** decolorization over time in presence of ZnO nanoparticle catalyst.

4.4.1.1 Comparison of selective Catalysts

The photocatalytic activities of selected ZnO catalysts were evaluated their influence on MB photodegradation was investigated via kinetic profiles, under operating conditions. Samples tested includes full series of nanoparticle catalyst prepared from acetate salt precursor and heat-treated samples. Also, tested were the highest and lowest temperature synthesized nanoparticles from sulphate (ZS-55 and ZS-70) and nitrate (ZN-55 and ZN-70) salt precursor.

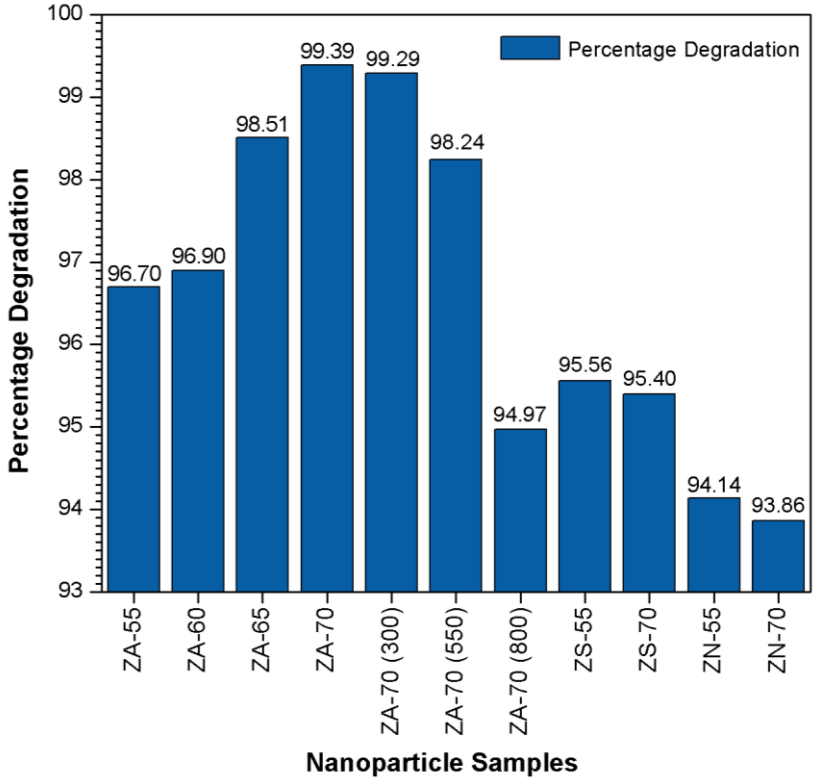

Fig. 4.4.2 Prepared ZnO Nanoparticle showing percentage degradation of methylene blue dye in 50min of irradiation time.

Fig. 4.4.2 shows that the highest photocatalytic activity is shown by samples prepared using acetate salt precursor, followed by sulphate and the lowest degradation activity is displayed by nanoparticles derived from nitrates salt precursor. Sample ZA-70 exhibits the best catalytic activity amongst all tested samples with the highest rate constant of $0.1 min^{-1}$ shown in Fig. 4.4.3 (c), effectively degrading 99.39% of methylene blue dye in 50 minutes. The sample ZA-70's superior photocatalytic activity, in comparison to other tested samples, is credited to:

- Highest defects concentration as shown by Photoluminesce results.
- Highest surface area for photocatalytic reaction because of smallest crystallite size of 21.1 nm.

Similarly, the photocatalysis results are well in accordance with the Photoluminesce results as all samples in ZA show highest density of defects followed by sulphates and nitrates samples. Furthermore, photocatalysis tests were also conducted for the ZA-70 sample which was further heat treated at 300°C, 550°C and 800°C. Results show that upon heat treatment the photocatalytic activity decreased and shows a trend that increase in heat treatment temperature decreases the photocatalytic activity because of decrease in defect concentration in ZnO nanoparticles.

Both tested samples via sulphate salt precursor (ZS-55 and ZS-70) have close values of percentage degradation, as is the case for tested nitrate derived particles (ZN-55 and ZN-70) because their Photoluminesce spectra is almost same in addition to the same crystallite size obtained via Xrd analysis.

The enhanced photocatalytic activity is attributed to presence of various defects in ZnO nanoparticle as confirmed by Photoluminesce. The presence of defects creates sub levels or intermediate bands within the bandgap which effectively trap electro-hole pair thus suppressing recombination process, which is a major limiting factor in photocatalytic activity.

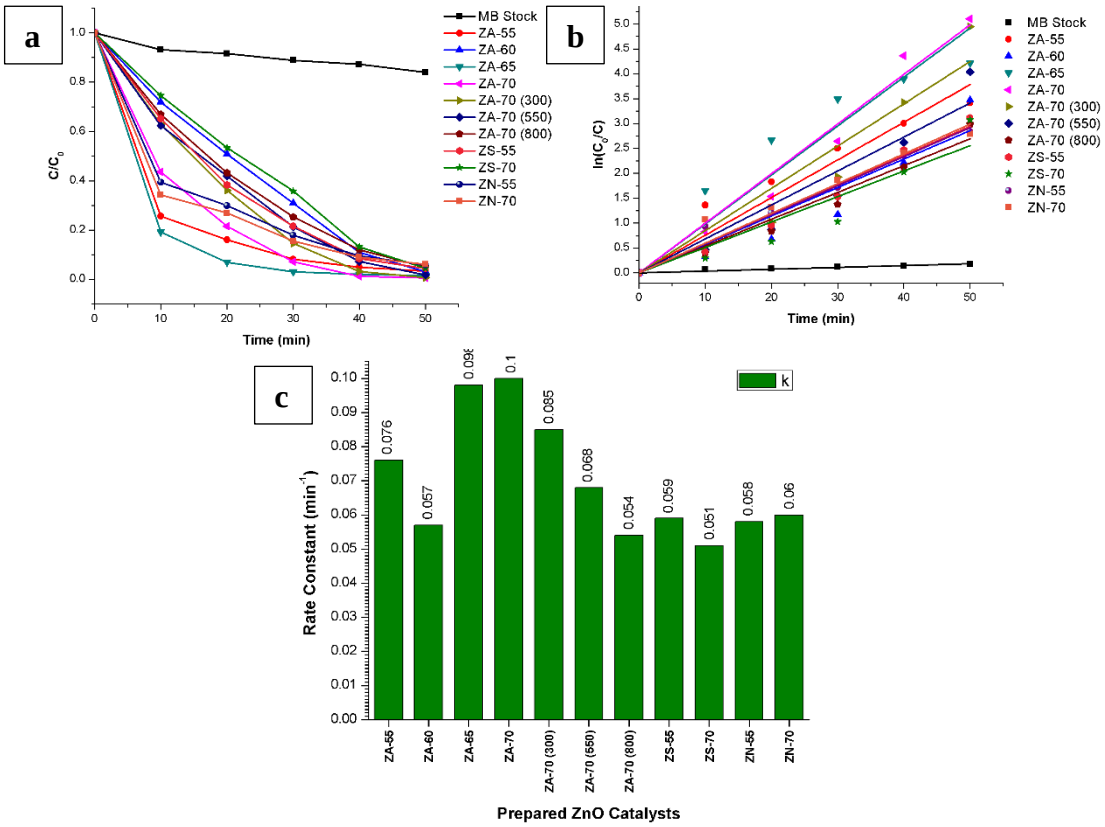

Fig. 4.4.3 Photocatalytic degradation profile of prepared nanoparticle catalysts, **(b)** their kinetic profile and **(c)** their rate constant in 50min.

4.4.1.2 Effect of pH

One of the most important parameters influencing photocatalysis is pH. The initial pH of MB stock solution was 5.98, which was varied by the addition of 1M NaOH or HCl to study the effect of pH on degradation rate. The pH of the dye solution was adjusted at different values of 1.85, 5.98, 8.20, 11.95 and 13.9, prior to irradiation. At higher pH values of 11.95 and 13.9, methylene blue self-degraded as shown by absorbance behavior in Fig. 4.4.4 and hence the reason why photocatalytic activity for these values couldn't be monitored.

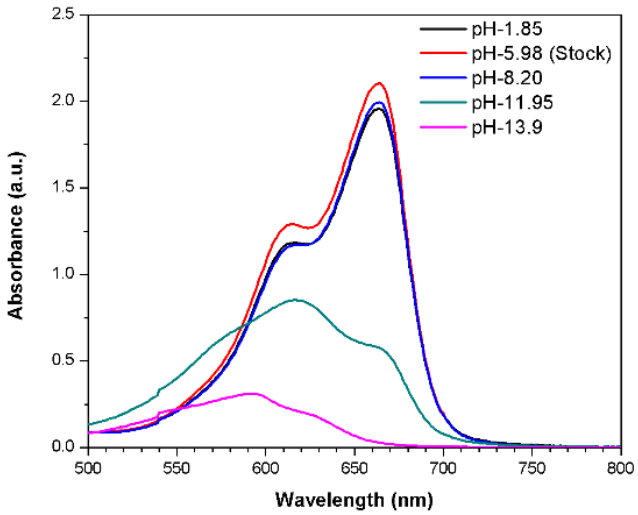

Fig. 4.4.4 MB dye absorbance as a function of pH.

Increase in pH favors the photocatalytic activity as shown in Fig. 4.4.5 (c). The rate constant is 0.049min^{-1}, 0.1min^{-1} and 0.095 min^{-1} for pH 1.85, 5.98, 8.20 respectively. At lower pH values, nanoparticles usually undergo dissolution in aqueous medium furthermore, in case of ZnO, nanoparticles become positively charged and due to repulsive interaction with cationic MB, there is decrease in MB adsorption leading to lower transfer rate resulting in relatively low photocatalytic activity. Aggregation in nanoparticles can decrease dissolution rates or can completely quench the process [114], as reported by Rubasinghege [115] for metal-containing nanorods in solution. So, this is possibly a reason why even at lower pH value of 1.85, prepared ZnO particles have been able to carry out MB degradation. Whereas, at higher pH values, ZnO catalyst is negatively charged with excess OH^-, which act as whole scavengers on its surface, initiating dye directly via photogenerated $^{\bullet}OH$ radicals and inhibiting particles dissolution. At even higher pH values, oxidizing species (e.g. $O_2^{\bullet-}$) are responsible for increased degradation of dye [56, 61].

Hence, the optimum pH value for prepared nanoparticles from range of pH 1.85 – pH 8.20. is pH 5.98, interestingly it is the default pH of MB stock solution as well.

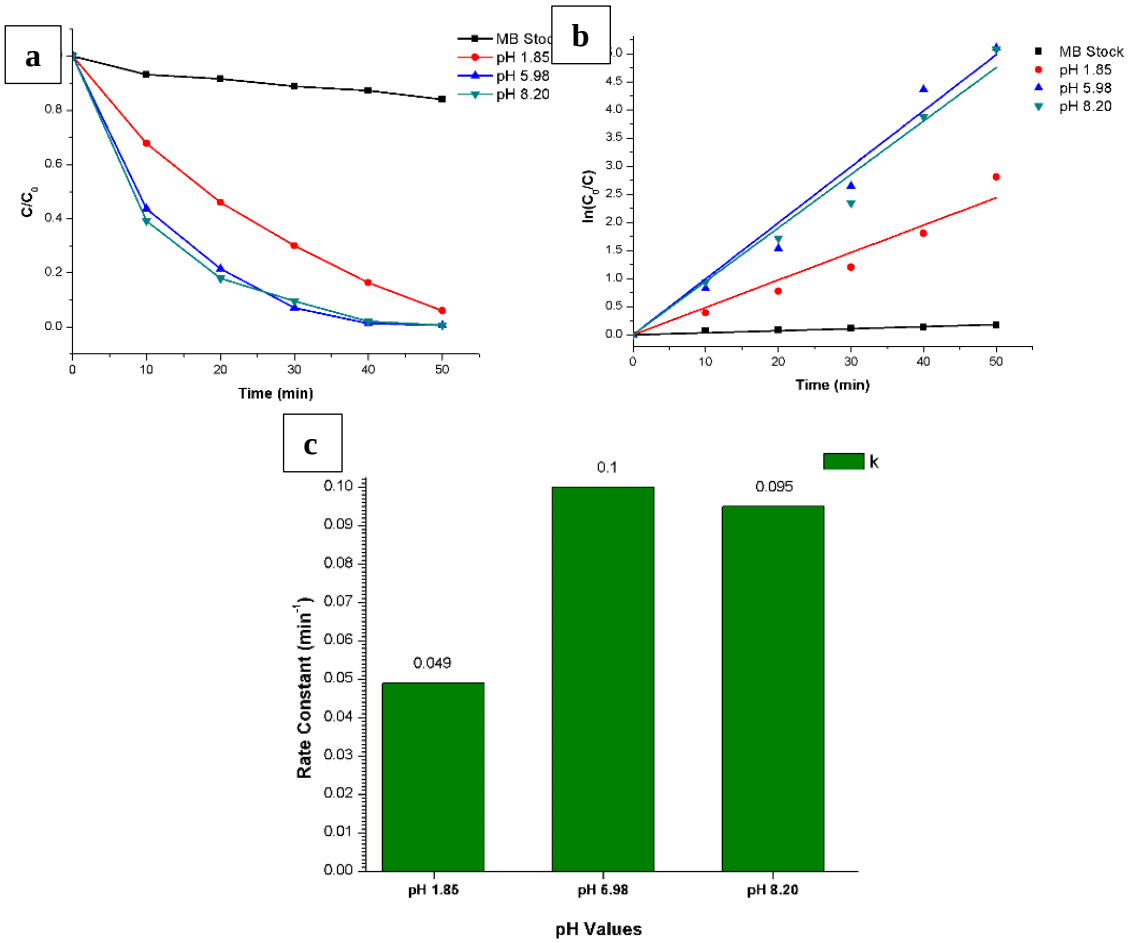

Fig. 4.4.5 (a) Photocatalytic degradation profile at different pH, **(b)** its kinetic profile and **(c)** its rate constant in 50min.

4.4.1.3 Effect of Catalyst Concentration

Fig. 4.4.6 shows the degradation profile at various catalyst concentrations. The catalyst loading was varied from 20mg up to 120mg in 60ml of MB stock solution. Results indicate increase in catalyst concentration increases the degradation rate and efficiency of photocatalytic reaction up to a certain point after which it again decreases. Rate constant for all concentrations are shown in Fig. 4.4.6 (c) and the lowest rate constant is 0.057min^{-1} for C20 and the highest is 0.109min^{-1} for C80. Since the percentage degradation for C40, C60, C80, C100 as shown in table 4.4 are very close to each other, the random behavior amongst them has been neglected as limitation of UV-Vis

absorption measurement. So, the optimum concentration is 80mg catalyst in 60ml of MB stock solution.

Increase in catalyst dosage provides more active sites because of increases the available active surface area for dye adsorption. However, after an optimum dose of catalyst the degradation decreases mainly due to the possibility of aggregation between particles as well as decline in light penetration owing to light scattering effect [56].

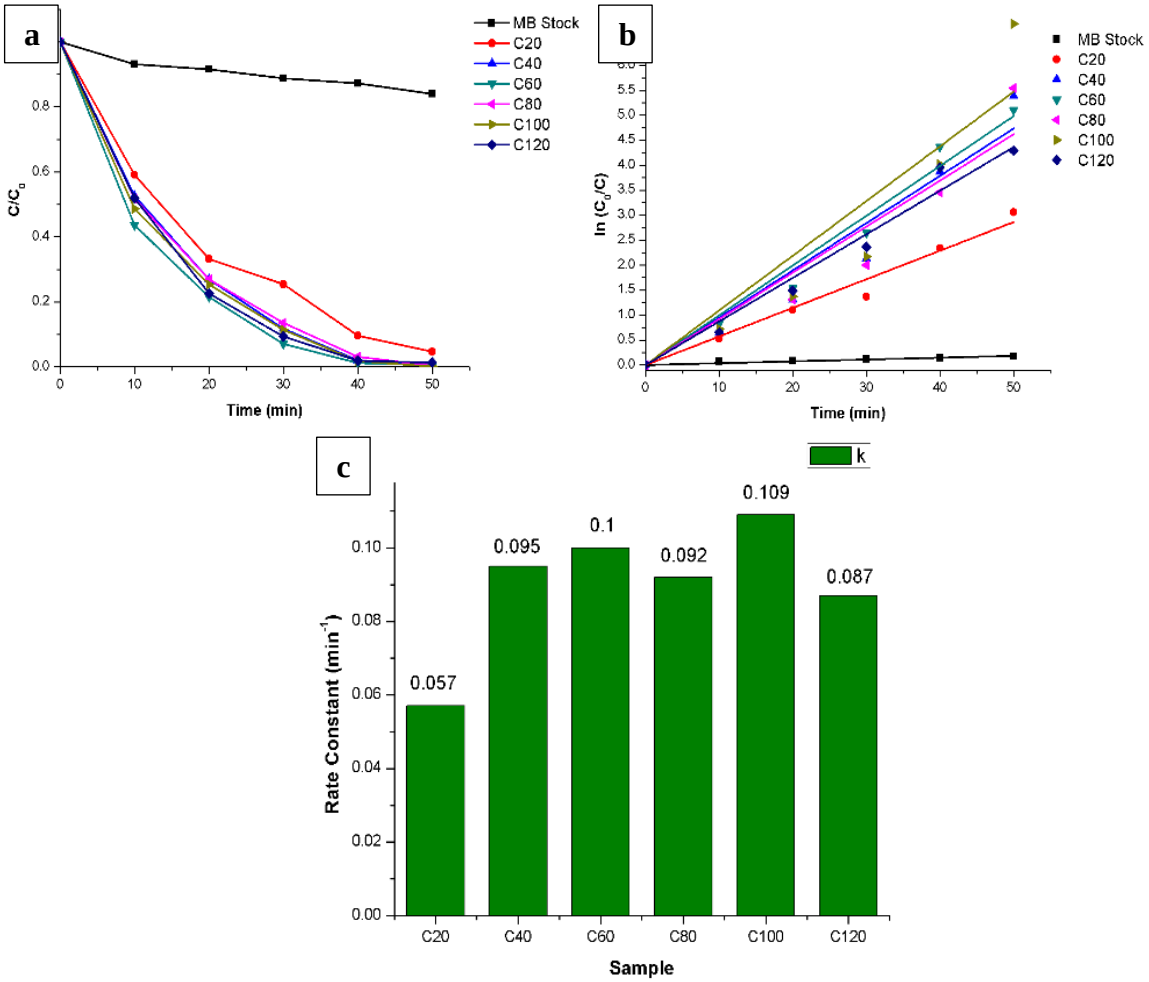

Fig. 4.4.6 (a) Photocatalytic degradation profile at different catalyst concentration, **(b)** its kinetic profile and **(c)** its rate constant in 50min.

Table 4.4 Linear correlation coefficient R^2, rate constant k and percentage degradation for photocatalytic degradation of methylene blue experiments.

	Sample	R^2	Rate Constant K (min^{-1})	Percentage Degradation
Tested Catalysts	MB	0.97	0.004	15.68
	ZA-55	0.98	0.076	96.70
	ZA-60	0.94	0.057	96.90
	ZA-65	0.96	0.098	98.51
	ZA-70	0.99	0.100	99.39
	ZA-70 (300)	0.96	0.085	99.29
	ZA-70 (550)	0.96	0.068	98.24
	ZA-70 (800)	0.98	0.054	94.97
	ZS-55	0.99	0.059	95.56
	ZS-70	0.94	0.051	95.40
	ZN-55	0.99	0.058	94.14
	ZN-70	0.98	0.060	93.86
Variation in pH for ZA-70	pH–1.85	0.98	0.049	93.98
	pH–5.98	0.99	0.100	99.39
	pH–8.20	0.99	0.095	99.38
Variation in Catalyst Concentration for ZA-70	C20	0.99	0.057	95.30
	C40	0.97	0.095	99.54
	C60	0.99	0.100	99.39
	C80	0.95	0.092	99.61
	C100	0.93	0.109	99.89
	C120	0.99	0.087	98.63

4.4.2 Rhodamine B Degradation

The photodegradation of rhodamine B dye was successfully carried out by sample ZA-70. Beer–Lambert law was used to calculate the relative concentration (C/C_0) of the RhB solution by the relative absorbance (A/A_0) at characteristic absorption peak of 554nm for RhB. Under dark conditions with the presence of catalyst RhB demonstrated very little dye degradation owing to adsorption of dye on the catalyst surface. Control experiments show that prepared samples degraded RhB dye as signified by decrease in the characteristic absorbance at 554nm and decolorization, as shown in fig. 4.4.7 (d). The decrease in absorption peak intensity is due to destruction of the dye chromogen. In addition, the hypsochromic shift of the absorption peak in the 480–600 nm region of the spectrum confirms the *N*-deethylation of RhB resulting in degradation and eventual mineralization [116]. The kinetic investigations were carried out by plotting $\ln(C/C_0)$ vs. irradiation time (t) for RhB which shows a good liner fit, with R^2 (correlation coefficients) value of 0.94, indicating pseudo-first-order kinetics followed by NPs for photodegradation. The calculated rate constant for ZA-

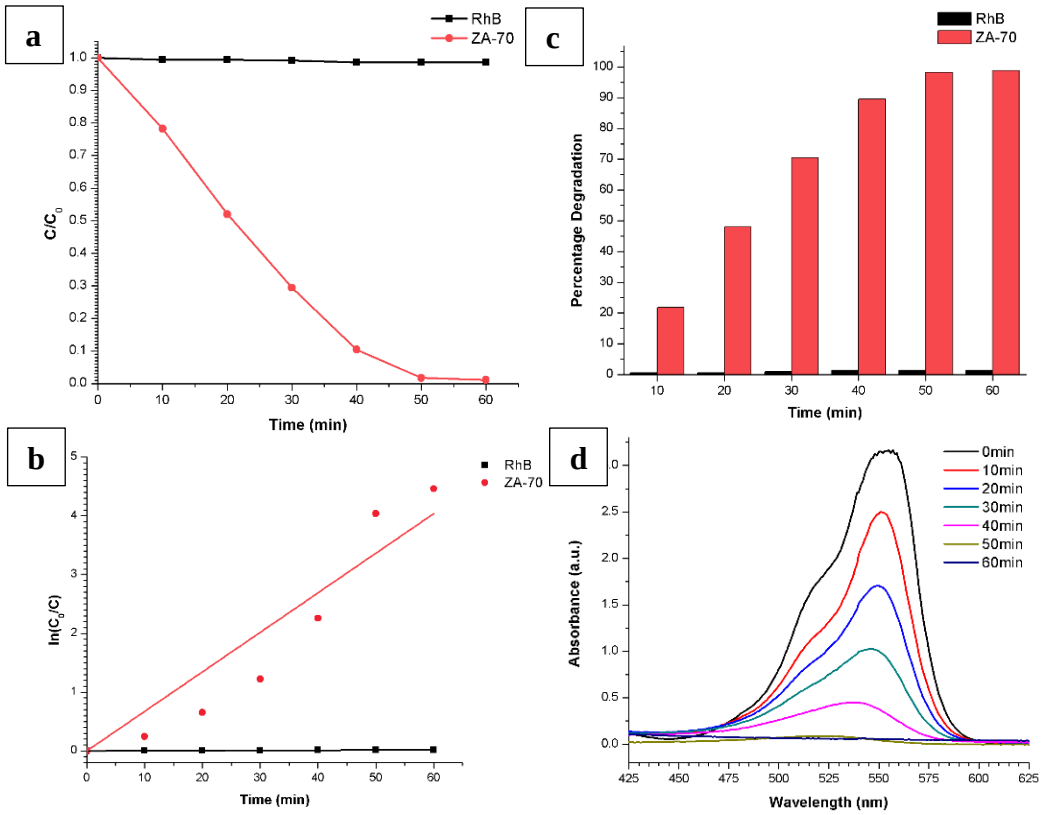

Fig. 4.4.7 (a) Photocatalytic degradation profile of Rhodamine B, **(b)** its kinetic profile and **(c)** its degradation efficiency **(d)** decrease in characteristic peak (554nm) in presence of ZA-70 catalyst for 60 min time.

70 is 0.067min^{-1} degrading 98.85% of RhB in 1 hour. Whereas, RhB solution showed only 1.39% of degradation without catalyst in the visible light.

4.4.3 Photodegradation Mechanism

The visible light photodegradation of both the organic dyes, MB and Rhodamine B can occurs either by:

i. Electron-hole pair generation upon light absorption by ZnO nanoparticles.
ii. Photosensitization because both MB and Rhodamine B show tendency to get excited under visible light.

The reaction involved in photocatalysis degradation hence involves both the above mention cases and are summarized below [55, 56, 61, 117].

First case will only happen if ZnO catalyst is visible active. And according to our optical results we have seen that prepared nanoparticles indeed visible region active because of high defects. Hence, upon irradiation of light source electrons jump from the valence band to the conduction band leaving holes in their wake and hence this give rise electron–hole pairs (equ.1).

$$ZnO + h\nu \longrightarrow ZnO\ (e^{-} \text{ in CB} + h^{+} \text{ in VB}) \quad (1)$$

Holes have a tendency to oxidize either water molecules (equ.2) or hydroxyl ion OH^{-} (equ.3) to produce hydroxyl radicals ($^{\bullet}OH$), a powerful radical that let alone can attacks the aromatic dye structure hence mineralizing the organic dye (equ.4).

$$\text{hole } (h^{+}) + H_2O \longrightarrow {}^{\bullet}OH + H^{+} \quad (2)$$

$$\text{hole } (h^{+}) + OH^{-} \longrightarrow {}^{\bullet}OH \quad (3)$$

$$^{\bullet}OH + \text{R-H} \longrightarrow R^{\bullet} + H_2O \quad (4)$$

or it can directly cause oxidation of the $>N(CH_3)_2$ substituted groups (eu.5),

$$\text{hole } (h^{+}) + R \longrightarrow R^{+\bullet} \longrightarrow \text{Intermediates} \quad (5)$$

Whereas, electrons in conduction band have the potential to reduce a substance such as reaction with molecular oxygen (O_2) reducing it to superoxide anion radical ($O_2^{\bullet -}$) (equ.6) which further reacts to form hydrogen peroxide H_2O_2 (equ.7 and equ.8).

$$\text{electron } (e^{-}) + O_2 \longrightarrow O_2^{\bullet -} \quad (6)$$

$$O_2^{\bullet-} + H^+ \longrightarrow HO_2^{\bullet} + O_2^{\bullet-} \longrightarrow HO_2^{\bullet} + O^- \quad (7)$$

$$2HO_2^{\bullet} \longrightarrow H_2O_2 + O_2 \quad (8)$$

$$H_2O_2 + O_2^{\bullet} \longrightarrow {}^{\bullet}OH + OH^- + O_2 \quad (9)$$

As, MB in visible light is susceptible to photosensitized degradation so imperative to mention it as well. In photosensitization phenomenon, visible irradiation excites MB and this photoexcited MB interacts with ground state catalyst. As a result, electrons from excited MB transfer to the conduction band of ZnO particles where surface oxygen traps them effectively suppressing the recombination of electronic-cationic radicals. The oxidized MB radicals, generated via electron injection, are unstable and decompose into bleached intermediate products as follows [68, 118]:

$$\text{Dye} + h\upsilon \rightarrow MB^* \quad (10)$$

$$\text{Dye}^* + ZnO \rightarrow \text{Dye}^{\bullet+} + ZnO(e^-) \quad (12)$$

$$ZnO(e^-) + O_2 \rightarrow ZnO + O_2^{\bullet-} \quad (13)$$

$$2H^+ + ZnO + O_2^{\bullet-} \rightarrow H_2O_2 \quad (14)$$

$$H_2O_2 + ZnO(e^-) \rightarrow {}^{\bullet}OH + OH^- \quad (15)$$

$$MB^{\bullet+} + O_2 \text{ (or } O_2^{\bullet-} \text{ or } {}^{\bullet}OH) \rightarrow \text{ peroxylated or hydroxylated (intermediates)} \quad (16)$$

And finally, these intermediates degraded into H_2O and CO_2.

In light of above-mentioned process, role of defects is critical in photocatalytic activity of a catalyst. As mentioned earlier, the defects create intermediate levels within the bandgap hence can capture an electron or a hole effectively preventing recombination. If a defect level grabs an electron than its associated VB hole takes part in catalysis. On the contrary CB electron participates in catalytic reaction if a hole is retained in a defect. Furthermore, after a certain degree of defect density is achieved, additional increase in defect concentration does not affect photocatalytic activity [72].

There exists a good agreement between Photoluminesce results and the photocatalytic activity shown by the prepared nanoparticles. The photocatalytic activities observed for all samples is of the same order as the trend shown in PL spectral intensity. The same order for both PL and PCA is attributed to the existence of defects concentration

in a sample. The sample with highest visible region PL intensity will have more oxygen related defects and will subsequently show highest photocatalytic activity.

Conclusions

ZnO nanoparticle were successfully synthesis using acetate, sulphate and nitrate salt precursor at 55°C, 60°C, 65°C and 70°C via coprecipitation method. The synthesis setup was equipped with oil bath and reflux setup. Spherical nanoparticles ranging from 20nm to 70nm were obtained with narrower bandgap energies than the bulk ZnO. The acetate salt precursor at 70°C yielded the smallest nanoparticles of 20nm size with the highest defect density revealed via photoluminescence spectra as well as showed highest percentage degradation of 99.39% of MB dye. The prepared nanoparticles exhibited green, yellow and red emission due to presence of defects such as oxygen vacancy, surface hydroxyl group and lattice dislocations respectively. Further heat treatment of prepared nanoparticles improved the violet emission reducing the visible region defects concentration. The green region defects remained, to a fairly certain degree, even after heat treatment up to 800°C of ZA-70 sample still displayed 94% MB photodegradation. Hence, it is the green region defect that plays major contribution in the enhanced photocatalytic activity. Sample prepared via acetate salt precursor showed highest photocatalytic activities followed by sulphate and then nitrate salt precursor. In addition, all of the prepared samples were able to degrade more than 93% of MB dye despite differences in synthesis parameter, so the described synthesis setup is ideal for defect driven growth of nanoparticles and their subsequent visible light activity. Visible light photocatalytic activity of ZA-70 was further tested using RhB dye and the results shows excellent activity of 98.85% degradation in one hour.

Recommendations

The research has room for further improvement, thus aspects for future work includes:

- Nanoparticles production via synthesis method described in this research can be commercialized by scaling up their yield.
- Thermodynamics and reaction kinetics involved in the synthesis process needs further investigation.
- Comprehensive explanations and related reasoning regarding role of salt precursor on physiochemical properties of nanoparticle is still needed. Hence chemistry of involved salt precursor should be studied in depth.
- Improvement in lab scale photocatalytic setup by using advance light sources and incorporating various components for better control over physical parameters such as light intensity, temperature.
- Nanoparticles removal from treated water, is extremely critical and is a research topic in its own right therefore, new methods are needed to be devised for their complete removal.

References

[1] B. Murty, P. Shankar, B. Raj, B. Rath, and J. Murday, *Textbook of nanoscience and nanotechnology*: Springer Science & Business Media, 2013.

[2] C. P. Poole Jr and F. J. Owens, *Introduction to nanotechnology*: John Wiley & Sons, 2003.

[3] V. Pokropivny, R. Lohmus, I. Hussainova, A. Pokropivny, and S. Vlassov, *Introduction to nanomaterials and nanotechnology*: Tartu University Press Ukraine, 2007.

[4] J. N. Tiwari, R. N. Tiwari, and K. S. Kim, "Zero-dimensional, one-dimensional, two-dimensional and three-dimensional nanostructured materials for advanced electrochemical energy devices," *Progress in Materials Science,* vol. 57, pp. 724-803, 2012.

[5] S. Salaheldeen Elnashaie, F. Danafar, and H. Hashemipour Rafsanjani, "From Nanotechnology to Nanoengineering," in *Nanotechnology for Chemical Engineers*, ed Singapore: Springer Singapore, 2015, pp. 79-178.

[6] R. Ameta and S. C. Ameta, *Photocatalysis: Principles and Applications*: Crc Press, 2016.

[7] S. C. Ameta and R. Ameta, *Green Chemistry: Fundamentals and Applications*: CRC press, 2013.

[8] H. M. a. Ü. Özgür, "General Properties of ZnO," in *Zinc Oxide: Fundamentals, Materials and Device Technology*, ed, 2009.

[9] T. Hanada, "Basic properties of ZnO, GaN, and related materials," *Oxide and nitride semiconductors*, pp. 1-19, 2009.

[10] Z. L. Wang, "Zinc oxide nanostructures: growth, properties and applications," *Journal of Physics: Condensed Matter,* vol. 16, pp. R829-R858, Jun 30 2004.

[11] A. Moezzi, "Zinc oxide: new insights into a material for all ages," 2012.

[12] Z. Guo and L. Tan, *Fundamentals and applications of nanomaterials*: Artech House, 2009.

[13] B. L. Cushing, V. L. Kolesnichenko, and C. J. O'Connor, "Recent advances in the liquid-phase syntheses of inorganic nanoparticles," *Chem Rev,* vol. 104, pp. 3893-946, Sep 2004.

[14] S. Salaheldeen Elnashaie, F. Danafar, and H. Hashemipour Rafsanjani, "Learning Synergism in Nanotechnology and Chemical Engineering by Case Study," in *Nanotechnology for Chemical Engineers*, ed Singapore: Springer Singapore, 2015, pp. 179-272.

[15] A. K. Srivastava, *Oxide nanostructures: Growth, microstructures, and properties*: Pan Stanford, 2014.

[16] J. Rodrıguez-Paez, A. Caballero, M. Villegas, C. Moure, P. Duran, and J. Fernandez, "Controlled precipitation methods: formation mechanism of ZnO nanoparticles," *Journal of the European Ceramic Society,* vol. 21, pp. 925-930, 2001.

[17] A. Moezzi, M. Cortie, and A. McDonagh, "Aqueous pathways for the formation of zinc oxide nanoparticles," *Dalton Trans,* vol. 40, pp. 4871-8, May 14 2011.

[18] V. Koutu, L. Shastri, and M. Malik, "Effect of NaOH concentration on optical properties of zinc oxide nanoparticles," *Materials Science-Poland,* vol. 34, pp. 819-827, 2016.

[19] K. Swaroop and H. Somashekarappa, "Effect of pH values on surface Morphology and Particle size variation in ZnO Nanoparticles Synthesised by co-precipitation Method," *Research Journal of Recent Sciences,* vol. 2277, p. 2502, 2015.

[20] M. Jay Chithra, M. Sathya, and K. Pushpanathan, "Effect of pH on Crystal Size and Photoluminescence Property of ZnO Nanoparticles Prepared by Chemical Precipitation Method," *Acta Metallurgica Sinica (English Letters),* vol. 28, pp. 394-404, 2015.

[21] U. Manzoor, F. Tuz Zahra, S. Rafique, M. T. Moin, and M. Mujahid, "Effect of Synthesis Temperature, Nucleation Time, and Postsynthesis Heat Treatment of ZnO Nanoparticles and Its Sensing Properties," *Journal of Nanomaterials,* vol. 2015, pp. 1-6, 2015.

[22] U. Manzoor, M. Islam, L. Tabassam, and S. U. Rahman, "Quantum confinement effect in ZnO nanoparticles synthesized by co-precipitate method," *Physica E: Low-dimensional Systems and Nanostructures,* vol. 41, pp. 1669-1672, Sep 2009.

[23] S. Sepulveda-Guzman, B. Reeja-Jayan, E. de La Rosa, A. Torres-Castro, V. Gonzalez-Gonzalez, and M. Jose-Yacaman, "Synthesis of assembled ZnO

structures by precipitation method in aqueous media," *Materials Chemistry and Physics*, vol. 115, pp. 172-178, 2009.

[24] J. J. Richardson and F. F. Lange, "Controlling low temperature aqueous synthesis of ZnO. 1. Thermodynamic analysis," *Crystal Growth and Design*, vol. 9, pp. 2570-2575, 2009.

[25] C. K. Srikanth and P. Jeevanandam, "Effect of anion on the homogeneous precipitation of precursors and their thermal decomposition to zinc oxide," *Journal of Alloys and Compounds*, vol. 486, pp. 677-684, Nov 3 2009.

[26] P. S. Kumar and A. S. Nesaraj, "Effect of the precursor salts on the wet chemical synthesis of ZnO nanoparticles," *synthesis*, vol. 17, p. 18, 2015.

[27] M. Pudukudy and Z. Yaakob, "Simple chemical synthesis of novel ZnO nanostructures: Role of counter ions," *Solid State Sciences*, vol. 30, pp. 78-88, Apr 2014.

[28] N. Rathore and S. K. Sarkar, "Effect of Different Anions on ZnO Morphology," *Energy Procedia*, vol. 54, pp. 771-776, 2014.

[29] N. S. Rao and M. V. B. Rao, "Structural and Optical Investigation of ZnO Nanopowders Synthesized from Zinc Chloride and Zinc Nitrate," *American Journal of Materials Science*, vol. 5, pp. 66-68, 2015.

[30] L. Kumar Jangir, Y. Kumari, A. Kumar, M. Kumar, and K. Awasthi, "Investigation of luminescence and structural properties of ZnO nanoparticles, synthesized with different precursors," *Materials Chemistry Frontiers*, vol. 1, pp. 1413-1421, 2017.

[31] S. Y. Purwaningsih, S. Pratapa, Triwikantoro, and Darminto, "Synthesis of nano-sized ZnO particles by co-precipitation method with variation of heating time," vol. 1708, p. 030040, 2016.

[32] S. Sugapriya, S. Lakshmi, and C. Senthilkumaran, "Effect on Annealing Temperature on ZnO Nanoparticles," *International Journal of ChemTech Research*, vol. 8, pp. 297-302, 2015.

[33] S. Kumar and P. D. Sahare, "Effects of Annealing on the Surface Defects of Zinc Oxide Nanoparticles," *Nano*, vol. 07, p. 1250022, 2012.

[34] M. K. Kavitha, K. B. Jinesh, R. Philip, P. Gopinath, and H. John, "Defect engineering in ZnO nanocones for visible photoconductivity and nonlinear absorption," *Phys Chem Chem Phys*, vol. 16, pp. 25093-100, Dec 7 2014.

[35] D. Raoufi, "Synthesis and microstructural properties of ZnO nanoparticles prepared by precipitation method," *Renewable Energy,* vol. 50, pp. 932-937, Feb 2013.

[36] R. Raji and K. Gopchandran, "ZnO nanostructures with tunable visible luminescence: Effects of kinetics of chemical reduction and annealing," *Journal of Science: Advanced Materials and Devices,* vol. 2, pp. 51-58, 2017.

[37] N. Han, X. Wu, L. Chai, H. Liu, and Y. Chen, "Counterintuitive sensing mechanism of ZnO nanoparticle based gas sensors," *Sensors and Actuators B: Chemical,* vol. 150, pp. 230-238, 2010/09/21/ 2010.

[38] D. R. Hang, S. E. Islam, K. H. Sharma, S. W. Kuo, C. Z. Zhang, and J. J. Wang, "Annealing effects on the optical and morphological properties of ZnO nanorods on AZO substrate by using aqueous solution method at low temperature," *Nanoscale Res Lett,* vol. 9, p. 632, 11/25 2014.

[39] L. P. Etcheverry, W. H. Flores, D. L. d. Silva, and E. C. Moreira, "Annealing Effects on the Structural and Optical Properties of ZnO Nanostructures," *Materials Research,* vol. 21, 2018.

[40] J. Wang, R. Chen, Y. Xia, G. Wang, H. Zhao, L. Xiang, *et al.*, "Cost-effective large-scale synthesis of oxygen-defective ZnO photocatalyst with superior activities under UV and visible light," *Ceramics International,* vol. 43, pp. 1870-1879, 2017.

[41] Z. Pei, L. Ding, J. Hu, S. Weng, Z. Zheng, M. Huang, *et al.*, "Defect and its dominance in ZnO films: A new insight into the role of defect over photocatalytic activity," *Applied Catalysis B: Environmental,* vol. 142, pp. 736-743, 2013.

[42] A. Djurišić, Y. Leung, K. Tam, Y. Hsu, L. Ding, W. Ge, *et al.*, "Defect emissions in ZnO nanostructures," *Nanotechnology,* vol. 18, p. 095702, 2007.

[43] N. S. Han, H. S. Shim, J. H. Seo, S. Y. Kim, S. M. Park, and J. K. Song, "Defect states of ZnO nanoparticles: Discrimination by time-resolved photoluminescence spectroscopy," *Journal of Applied Physics,* vol. 107, p. 084306, Apr 15 2010.

[44] K. H. Tam, C. K. Cheung, Y. H. Leung, A. B. Djurisic, C. C. Ling, C. D. Beling, *et al.*, "Defects in ZnO nanorods prepared by a hydrothermal method," *J Phys Chem B,* vol. 110, pp. 20865-71, Oct 26 2006.

[45] B. Cao, X. Teng, S. H. Heo, Y. Li, S. O. Cho, G. Li, *et al.*, "Different ZnO nanostructures fabricated by a seed-layer assisted electrochemical route and their photoluminescence and field emission properties," *The Journal of Physical Chemistry C*, vol. 111, pp. 2470-2476, 2007.

[46] S. Kim, R. M. D. S. Somaratne, and J. E. Whitten, "Effect of Adsorption on the Photoluminescence of Zinc Oxide Nanoparticles," *The Journal of Physical Chemistry C*, vol. 122, pp. 18982-18994, 2018/08/23 2018.

[47] W.-Y. Wu, W.-Y. Kung, and J.-M. Ting, "Effect of pH Values on the Morphology of Zinc Oxide Nanostructures and their Photoluminescence Spectra," *Journal of the American Ceramic Society*, vol. 94, pp. 699-703, Mar 2011.

[48] A. T. Do, H. T. Giang, T. T. Do, N. Q. Pham, and G. T. Ho, "Effects of palladium on the optical and hydrogen sensing characteristics of Pd-doped ZnO nanoparticles," *Beilstein J Nanotechnol*, vol. 5, pp. 1261-7, 2014.

[49] N. Padmavathy and R. Vijayaraghavan, "Enhanced bioactivity of ZnO nanoparticles-an antimicrobial study," *Sci Technol Adv Mater*, vol. 9, p. 035004, Jul 2008.

[50] I. Ozerov, M. Arab, V. I. Safarov, W. Marine, S. Giorgio, M. Sentis, *et al.*, "Enhancement of exciton emission from ZnO nanocrystalline films by pulsed laser annealing," *Applied surface science*, vol. 226, pp. 242-248, 2004.

[51] Y. Wang, S. Lau, X. Zhang, H. Hng, H. Lee, S. Yu, *et al.*, "Enhancement of near-band-edge photoluminescence from ZnO films by face-to-face annealing," *Journal of crystal growth*, vol. 259, pp. 335-342, 2003.

[52] M. Willander, O. Nur, J. R. Sadaf, M. I. Qadir, S. Zaman, A. Zainelabdin, *et al.*, "Luminescence from Zinc Oxide Nanostructures and Polymers and their Hybrid Devices," *Materials*, vol. 3, pp. 2643-2667, Apr 2010.

[53] U. I. Gaya, *Heterogeneous photocatalysis using inorganic semiconductor solids*: Springer Science & Business Media, 2013.

[54] M. Pirhashemi, A. Habibi-Yangjeh, and S. R. Pouran, "Review on the criteria anticipated for the fabrication of highly efficient ZnO-based visible-light-driven photocatalysts," *Journal of industrial and engineering chemistry*, 2018.

[55] L. V. Bora and R. K. Mewada, "Visible/solar light active photocatalysts for organic effluent treatment: Fundamentals, mechanisms and parametric

review," *Renewable and Sustainable Energy Reviews,* vol. 76, pp. 1393-1421, Sep 2017.

[56] S.-M. Lam, J.-C. Sin, A. Z. Abdullah, and A. R. Mohamed, "Degradation of wastewaters containing organic dyes photocatalysed by zinc oxide: a review," *Desalination and Water Treatment,* vol. 41, pp. 131-169, 2012.

[57] S. Ahmed, M. Rasul, W. N. Martens, R. Brown, and M. Hashib, "Advances in heterogeneous photocatalytic degradation of phenols and dyes in wastewater: a review," *Water, Air, & Soil Pollution,* vol. 215, pp. 3-29, 2011.

[58] T. M. Elmorsi, M. H. Elsayed, and M. F. Bakr, "Enhancing the removal of methylene blue by modified ZnO nanoparticles: kinetics and equilibrium studies," *Canadian Journal of Chemistry,* vol. 95, pp. 590-600, May 2017.

[59] S. Baruah, S. S. Sinha, B. Ghosh, S. K. Pal, A. K. Raychaudhuri, and J. Dutta, "Photoreactivity of ZnO nanoparticles in visible light: Effect of surface states on electron transfer reaction," *Journal of Applied Physics,* vol. 105, p. 074308, Apr 1 2009.

[60] K. Byrappa, A. K. Subramani, S. Ananda, K. M. L. Rai, R. Dinesh, and M. Yoshimura, "Photocatalytic degradation of rhodamine B dye using hydrothermally synthesized ZnO," *Bulletin of Materials Science,* vol. 29, pp. 433-438, October 01 2006.

[61] M. A. Islam, I. A. Siddiquey, M. A. R. Khan, M. M. Alam, S. S. Islam, and M. A. Hasnat, "Adsorption and UV-Visible Light Induced Degradation of Methylene Blue over ZnO Nano-Particles," *International Journal of Chemical Reactor Engineering,* vol. 9, 2011.

[62] T. Bora, P. Sathe, K. Laxman, S. Dobretsov, and J. Dutta, "Defect engineered visible light active ZnO nanorods for photocatalytic treatment of water," *Catalysis Today,* vol. 284, pp. 11-18, 2017/04/15/ 2017.

[63] X. Zhang, J. Qin, Y. Xue, P. Yu, B. Zhang, L. Wang, *et al.*, "Effect of aspect ratio and surface defects on the photocatalytic activity of ZnO nanorods," *Sci Rep,* vol. 4, p. 4596, Apr 4 2014.

[64] W. Raza, S. M. Faisal, M. Owais, D. Bahnemann, and M. Muneer, "Facile fabrication of highly efficient modified ZnO photocatalyst with enhanced photocatalytic, antibacterial and anticancer activity," *RSC Advances,* vol. 6, pp. 78335-78350, 2016.

[65] W. He, H. K. Kim, W. G. Wamer, D. Melka, J. H. Callahan, and J. J. Yin, "Photogenerated charge carriers and reactive oxygen species in ZnO/Au hybrid nanostructures with enhanced photocatalytic and antibacterial activity," *J Am Chem Soc,* vol. 136, pp. 750-7, Jan 15 2014.

[66] Y. Peng, Y. Wang, Q.-G. Chen, Q. Zhu, and A. W. Xu, "Stable yellow ZnO mesocrystals with efficient visible-light photocatalytic activity," *CrystEngComm,* vol. 16, pp. 7906-7913, 2014.

[67] S. Baruah, R. F. Rafique, and J. Dutta, "Visible Light Photocatalysis by Tailoring Crystal Defects in Zinc Oxide Nanostructures," *Nano,* vol. 3, pp. 399-407, Oct 2008.

[68] S. Akir, A. Barras, Y. Coffinier, M. Bououdina, R. Boukherroub, and A. D. Omrani, "Eco-friendly synthesis of ZnO nanoparticles with different morphologies and their visible light photocatalytic performance for the degradation of Rhodamine B," *Ceramics International,* vol. 42, pp. 10259-10265, 2016.

[69] Y. Choi and Y.-I. Lee, "Facile and Selective Synthesis of ZnO Hollow or Crumpled Spheres and Their Photocatalytic Degradation Activities," *Journal of the Korean Ceramic Society,* vol. 55, pp. 261-266, 5 2018.

[70] S. Steplin Paul Selvin, A. Ganesh Kumar, L. Sarala, R. Rajaram, A. Sathiyan, J. Princy Merlin, *et al.*, "Photocatalytic Degradation of Rhodamine B Using Zinc Oxide Activated Charcoal Polyaniline Nanocomposite and Its Survival Assessment Using Aquatic Animal Model," *ACS Sustainable Chemistry & Engineering,* vol. 6, pp. 258-267, 2018/01/02 2017.

[71] A. M. Pourrahimi, D. Liu, L. K. H. Pallon, R. L. Andersson, A. Martínez Abad, J. M. Lagarón, *et al.*, "Water-based synthesis and cleaning methods for high purity ZnO nanoparticles – comparing acetate, chloride, sulphate and nitrate zinc salt precursors," *RSC Adv.,* vol. 4, pp. 35568-35577, 2014.

[72] F. Kayaci, S. Vempati, I. Donmez, N. Biyikli, and T. Uyar, "Role of zinc interstitials and oxygen vacancies of ZnO in photocatalysis: a bottom-up approach to control defect density," *Nanoscale,* vol. 6, pp. 10224-34, Sep 7 2014.

[73] P. Bindu and S. Thomas, "Estimation of lattice strain in ZnO nanoparticles: X-ray peak profile analysis," *Journal of Theoretical and Applied Physics,* vol. 8, pp. 123-134, 2014.

[74] A. Khorsand Zak, W. H. Abd. Majid, M. E. Abrishami, and R. Yousefi, "X-ray analysis of ZnO nanoparticles by Williamson–Hall and size–strain plot methods," *Solid State Sciences,* vol. 13, pp. 251-256, 2011/01/01/ 2011.

[75] F. Meng, S. A. Morin, A. Forticaux, and S. Jin, "Screw dislocation driven growth of nanomaterials," *Acc Chem Res,* vol. 46, pp. 1616-26, Jul 16 2013.

[76] C.-C. Chen, C. Zhu, E. R. White, C.-Y. Chiu, M. C. Scott, B. C. Regan, *et al.*, "Three-dimensional imaging of dislocations in a nanoparticle at atomic resolution," *Nature,* vol. 496, p. 74, 03/27/online 2013.

[77] A. P. Lange, A. Samanta, H. Majidi, S. Mahajan, J. Ging, T. Y. Olson, *et al.*, "Dislocation mediated alignment during metal nanoparticle coalescence," *Acta Materialia,* vol. 120, pp. 364-378, 2016/11/01/ 2016.

[78] E. S. Kumar, C. Maneesh, F. Bellarmine, M. Ramanjaneyulu, N. Daisuke, H. Mitsuhiro, *et al.*, "Formation of one-dimensional ZnO nanowires from screw-dislocation-driven two-dimensional hexagonal stacking on diamond substrate using nanoparticle-assisted pulsed laser deposition," *Journal of Physics D: Applied Physics,* vol. 47, p. 034016, 2014.

[79] S. A. Morin, M. J. Bierman, J. Tong, and S. Jin, "Mechanism and kinetics of spontaneous nanotube growth driven by screw dislocations," *Science,* vol. 328, pp. 476-80, Apr 23 2010.

[80] S. A. Morin and S. Jin, "Screw dislocation-driven epitaxial solution growth of ZnO nanowires seeded by dislocations in GaN substrates," *Nano Lett,* vol. 10, pp. 3459-63, Sep 8 2010.

[81] Q. Ma, T. E. Saraswati, A. Ogino, and M. Nagatsu, "Improvement of UV emission from highly crystalline ZnO nanoparticles by pulsed laser ablation under O2/He glow discharge," *Applied Physics Letters,* vol. 98, p. 051908, 2011/01/31 2011.

[82] S. Y. Chen, P. Shen, and J. Jiang, "Polymorphic transformation of dense ZnO nanoparticles: implications for chair/boat-type Peierls distortions of AB semiconductor," *J Chem Phys,* vol. 121, pp. 11309-13, Dec 8 2004.

[83] J. Mujtaba, H. Sun, F. Fang, M. Ahmad, and J. Zhu, "Fine control over the morphology and photocatalytic activity of 3D ZnO hierarchical nanostructures: capping vs. etching," *RSC Advances,* vol. 5, pp. 56232-56238, 2015.

[84] S. Maiti, S. Pal, and K. K. Chattopadhyay, "Recent advances in low temperature, solution processed morphology tailored ZnO nanoarchitectures

for electron emission and photocatalysis applications," *CrystEngComm,* vol. 17, pp. 9264-9295, 2015.

[85] S. S. Alias and A. A. Mohamad, *Synthesis of zinc oxide by sol-gel method for photoelectrochemical cells*: Springer, 2014.

[86] Y. Zhang and M. Muhammed, "Critical evaluation of thermodynamics of complex formation of metal ions in aqueous solutions: VI. Hydrolysis and hydroxo-complexes of Zn2+ at 298.15 K," *Hydrometallurgy,* vol. 60, pp. 215-236, 2001.

[87] A. Degen and M. Kosec, "Effect of pH and impurities on the surface charge of zinc oxide in aqueous solution," *Journal of the European Ceramic Society,* vol. 20, pp. 667-673, May 2000.

[88] J. Zhang, L. Sun, J. Yin, H. Su, C. Liao, and C. Yan, "Control of ZnO morphology via a simple solution route," *Chemistry of Materials,* vol. 14, pp. 4172-4177, 2002.

[89] R. Viswanatha, H. Amenitsch, and D. D. Sarma, "Growth kinetics of ZnO nanocrystals: a few surprises," *J Am Chem Soc,* vol. 129, pp. 4470-5, Apr 11 2007.

[90] S. Anitha and S. Muthukumaran, "Microstructure, crystallographic and photoluminescence examination of Ni doped ZnO nanoparticles co-doped with Co by sol–gel method," *Journal of Materials Science: Materials in Electronics,* vol. 28, pp. 12995-13005, 2017.

[91] G. Xiong, U. Pal, J. G. Serrano, K. B. Ucer, and R. T. Williams, "Photoluminesence and FTIR study of ZnO nanoparticles: the impurity and defect perspective," *physica status solidi (c),* vol. 3, pp. 3577-3581, 2006.

[92] D. H. Williams and I. Fleming, *Spectroscopic Methods in Organic Chemistry*: McGraw-Hill, 2008.

[93] A. Sahai and N. Goswami, "Structural and vibrational properties of ZnO nanoparticles synthesized by the chemical precipitation method," *Physica E: Low-dimensional Systems and Nanostructures,* vol. 58, pp. 130-137, Apr 2014.

[94] A. M. Pourrahimi, D. Liu, V. Ström, M. S. Hedenqvist, R. T. Olsson, and U. W. Gedde, "Heat treatment of ZnO nanoparticles: new methods to achieve high-purity nanoparticles for high-voltage applications," *Journal of Materials Chemistry A,* vol. 3, pp. 17190-17200, 2015.

[95] H. Sutanto, S. Wibowo, I. Nurhasanah, E. Hidayanto, and H. Hadiyanto, "Ag Doped ZnO Thin Films Synthesized by Spray Coating Technique for Methylene Blue Photodegradation under UV Irradiation," *International Journal of Chemical Engineering,* vol. 2016, pp. 1-6, 2016.

[96] J. A. Soares, "Introduction to optical characterization of materials," in *Practical Materials Characterization,* ed: Springer, 2014, pp. 43-92.

[97] J. Wang, Z. Wang, B. Huang, Y. Ma, Y. Liu, X. Qin, *et al.*, "Oxygen vacancy induced band-gap narrowing and enhanced visible light photocatalytic activity of ZnO," *ACS Appl Mater Interfaces,* vol. 4, pp. 4024-30, Aug 2012.

[98] S. Mehmood, M. A. Rehman, H. Ismail, B. Mirza, and A. S. Bhatti, "Significance of postgrowth processing of ZnO nanostructures on antibacterial activity against gram-positive and gram-negative bacteria," *Int J Nanomedicine,* vol. 10, pp. 4521-33, 07/16 2015.

[99] Y. Chen, J. Jiang, Z. He, Y. Su, D. Cai, and L. Chen, "Growth mechanism and characterization of ZnO microbelts and self-assembled microcombs," *Materials Letters,* vol. 59, pp. 3280-3283, 2005.

[100] B. Jin and D. Wang, "Strong violet emission from zinc oxide dumbbell-like microrods and nanowires," *Journal of Luminescence,* vol. 132, pp. 1879-1884, 2012.

[101] O. Mekasuwandumrong, P. Pawinrat, P. Praserthdam, and J. Panpranot, "Effects of synthesis conditions and annealing post-treatment on the photocatalytic activities of ZnO nanoparticles in the degradation of methylene blue dye," *Chemical Engineering Journal,* vol. 164, pp. 77-84, 2010.

[102] A. S. Haja Hameed, C. Karthikeyan, S. Sasikumar, V. Senthil Kumar, S. Kumaresan, and G. Ravi, "Impact of alkaline metal ions Mg2+, Ca2+, Sr2+ and Ba2+ on the structural, optical, thermal and antibacterial properties of ZnO nanoparticles prepared by the co-precipitation method," *Journal of Materials Chemistry B,* vol. 1, p. 5950, 2013.

[103] X. Ding, Y. Fang, H. Qian, M. Zhao, W. Wang, J. Sha, *et al.*, "Influence of the precursor anion on the photoluminescence properties of ZnO," *Opt Express,* vol. 24, pp. 25876-25884, Oct 31 2016.

[104] J. Wang, P. Liu, X. Fu, Z. Li, W. Han, and X. Wang, "Relationship between oxygen defects and the photocatalytic property of ZnO nanocrystals in Nafion membranes," *Langmuir,* vol. 25, pp. 1218-23, Jan 20 2009.

[105] P. K. Sharma, A. C. Pandey, G. Zolnierkiewicz, N. Guskos, and C. Rudowicz, "Relationship between oxygen defects and the photoluminescence property of ZnO nanoparticles: a spectroscopic view," *Journal of Applied Physics,* vol. 106, p. 094314, 2009.

[106] S. Vempati, J. Mitra, and P. Dawson, "One-step synthesis of ZnO nanosheets: a blue-white fluorophore," *Nanoscale Res Lett,* vol. 7, p. 470, Aug 21 2012.

[107] G. K. Reddy, A. J. Reddy, R. H. Krishna, B. Nagabhushana, and G. R. Gopal, "Luminescence and spectroscopic investigations on Gd3+ doped ZnO nanophosphor," *Journal of Asian Ceramic Societies,* vol. 5, pp. 350-356, 2017.

[108] H. Kaftelen, K. Ocakoglu, R. Thomann, S. Tu, S. Weber, and E. Erdem, "EPR and photoluminescence spectroscopy studies on the defect structure of ZnO nanocrystals," *Physical Review B,* vol. 86, p. 014113, Jul 26 2012.

[109] A. S. Hameed, C. Karthikeyan, A. P. Ahamed, N. Thajuddin, N. S. Alharbi, S. A. Alharbi, *et al.*, "In vitro antibacterial activity of ZnO and Nd doped ZnO nanoparticles against ESBL producing Escherichia coli and Klebsiella pneumoniae," *Sci Rep,* vol. 6, p. 24312, Apr 13 2016.

[110] R. B. Cross, M. M. Souza, and E. M. Sankara Narayanan, "A low temperature combination method for the production of ZnO nanowires," *Nanotechnology,* vol. 16, pp. 2188-92, Oct 2005.

[111] M. Gomi, N. Oohira, K. Ozaki, and M. Koyano, "Photoluminescent and Structural Properties of Precipitated ZnO Fine Particles," *Japanese Journal of Applied Physics,* vol. 42, pp. 481-485, Feb 2003.

[112] R. Félix, M. Peres, S. Magalhães, M. R. Correia, A. Lourenço, T. Monteiro, *et al.*, "The Role of Edge Dislocations on the Red Luminescence of ZnO Films Deposited by RF-Sputtering," *Journal of Nanomaterials,* vol. 2015, pp. 1-11, 2015.

[113] A. B. Djurisic and Y. H. Leung, "Optical properties of ZnO nanostructures," *Small,* vol. 2, pp. 944-61, Aug 2006.

[114] S. W. Bian, I. A. Mudunkotuwa, T. Rupasinghe, and V. H. Grassian, "Aggregation and dissolution of 4 nm ZnO nanoparticles in aqueous environments: influence of pH, ionic strength, size, and adsorption of humic acid," *Langmuir,* vol. 27, pp. 6059-68, May 17 2011.

[115] G. Rubasinghege, R. W. Lentz, H. Park, M. M. Scherer, and V. H. Grassian, "Nanorod dissolution quenched in the aggregated state," *Langmuir*, vol. 26, pp. 1524-1527, 2009.

[116] R. Qiu, D. Zhang, Y. Mo, L. Song, E. Brewer, X. Huang, *et al.*, "Photocatalytic activity of polymer-modified ZnO under visible light irradiation," *J Hazard Mater*, vol. 156, pp. 80-5, Aug 15 2008.

[117] K. M. Lee, C. W. Lai, K. S. Ngai, and J. C. Juan, "Recent developments of zinc oxide based photocatalyst in water treatment technology: A review," *Water Res*, vol. 88, pp. 428-448, Jan 1 2016.

[118] J. Guo, J. Li, A. Yin, K. Fan, and W. Dai, "Photodegradation of Rhodamine B on Sulfur Doped ZnO/TiO2 Nanocomposite Photocatalyst under Visible-light Irradiation," *Chinese Journal of Chemistry*, vol. 28, pp. 2144-2150, 2010.